ANGLE OF ATTACK COMPUTATION SYSTEM

Duane B. Freeman

Sperry Rand Corporation

Prepared for:

Air Force Flight Dynamics Laboratory

September 1973

Unclassified

Security Classification

AD-771183

DOCUMENT CONTROL DATA - R & D

(Security classification of title, body of abstract and indexing annotation must be entered when the overall report is classified)

1. ORIGINATING ACTIVITY (Corporate author)	2a. REPORT SECURITY CLASSIFICATION
Sperry Flight Systems P.O. Box 21111 Phoenix, Arizona 85036	Unclassified 2b. GROUP –

3. REPORT TITLE

Angle of Attack Computation System

4. DESCRIPTIVE NOTES (Type of report and inclusive dates)

Final Report

5. AUTHOR(S) (First name, middle initial, last name)

Duane B. Freeman

6. REPORT DATE	7a. TOTAL NO. OF PAGES	7b. NO. OF REFS
September 1973	255	1

8a. CONTRACT OR GRANT NO.	9a. ORIGINATOR'S REPORT NUMBER(S)
F33615-71-C-1290 b. PROJECT NO. 8222 c. d.	71-0353-00-00 9b. OTHER REPORT NO(S) (Any other numbers that may be assigned this report)

10. DISTRIBUTION STATEMENT

Approved for public release; distribution unlimited.

11. SUPPLEMENTARY NOTES	12. SPONSORING MILITARY ACTIVITY
	Air Force Flight Dynamics Laboratory Air Force Systems Command Wright-Patterson Air Force Base, Ohio

13. ABSTRACT

The results of a program to evaluate computing angle-of-attack by inference using air data, aircraft acceleration, surface positions and stored aerodynamic data are presented in this report. The computation was implemented in an analog type airborne computer and evaluated in a U.S. Air Force RF-4C aircraft. The mathematical relationships selected for calculating the aircraft angle-of-attack, the system implementation and the flight test program are described herein. The flight test data is reduced, and computed angle-of-attack is compared to the output of an externally mounted vane. As indicated by the results, computed angle-of-attack is feasible and accurate with normally available onboard aircraft sensors.

DD FORM 1 NOV 65 1473

Unclassified

Security Classification

14. KEY WORDS	LINK A		LINK B		LINK C	
	ROLE	WT	ROLE	WT	ROLE	WT
Angle-of-Attack, Computed						

NOTICE

When Government drawings, specifications, or other data are used for any purpose other than in connection with a definitely related Government procurement operation, the United States Government thereby incurs no responsibility nor any obligation whatsoever; and the fact that the government may have formulated, furnished, or in any way supplied the said drawings, specifications, or other data, is not to be regarded by implication or otherwise as in any manner licensing the holder or any other person or corporation, or conveying any rights or permission to manufacture, use, or sell any patented invention that may in any way be related thereto.

Copies of this report should not be returned unless return is required by security considerations, contractual obligations, or notice on a specific document.

it

AFFDL-TR-73-89

ANGLE-OF-ATTACK COMPUTATION SYSTEM

DUANE B. FREEMAN

OCTOBER 1973

iC

FOREWORD

This report entitled "Angle-of-Attack Computation System" was prepared by Sperry Flight Systems, Phoenix, Arizona under USAF Contract Number F33615-71-C-1280. The contract was initiated under project number 8222, "Control Data Systems and Instrumentation Technology for Advanced Aerospace Military Vehicles", task number 822207, "Angle-of-Attack Processing System".

The work was administered under the direction of the Flight Control Division, Air Force Flight Dynamics Laboratory, Air Force Systems Command, Wright-Patterson Air Force Base, Ohio, Mr. John Houtz (AFFDL/FGL) Project Engineer.

GEORGE H. PURCELL, Acting Chief
Control Systems Development Branch
Flight Control Division
Air Force Flight Dynamics Laboratory

ABSTRACT

The results of a program to evaluate computing angle-of-attack by interference using air data, aircraft acceleration, surface positions and stored aerodynamic data are presented in this report. The computation was implemented in an analog type airborne computer and evaluated in a U.S. Air Force RF-4C aircraft. The mathematical relationships selected for calculating the aircraft angle-of-attack, the system implementation and the flight test program are described herein. The flight test data is reduced, and computed angle-of-attack is compared to the output of an externally mounted vane. As indicated by the results, computed angle-of-attack is feasible and accurate with normally available on-board aircraft sensors.

TABLE OF CONTENTS

LIST OF ILLUSTRATIONS

LIST OF TABLES

LIST OF SYMBOLS

Symbol	
g	Acceleration due to Earth Gravity
α	Angle-of-Attack
α_c	Output of Angle-of-Attack Processor
M	Mass of Aircraft
M'	Computed Mass of Aircraft
$\dot{M}'$	Computed Mass Rate
A_X	Output of Longitudinal Accelerometer
A_Z	Output of Normal Accelerometer
A_Y	Output of Lateral Accelerometer
a_z	$A_Z - g$
V_a	True Airspeed ($V_a = V_m$)
$\ddot{h}$	Vertical Acceleration
$\dot{h}$	Barometric Vertical Rate
h	Barometric Altitude
ρ	Air Density
q	Dynamic Pressure $\left(1/2\ \rho\ V_a^2\right)$
δ_s	Stabilator Position
δ_F	Flap Position
δ_a	Aileron Position
δ_T	Throttle Position
C_X	Longitudinal Force Coefficient $C_X = F_X/qS$
C_Z	Normal Force Coefficient $C_Z = F_Z/qS$
S	Wing Area
s	LaPlace Operator
τ	Time Constant
T	Thrust
λ_T	Thrust Line Incidence Angle
$C_{Z_{\delta_a}}$	Change in C_Z due to δ_a change

Symbol

$C_{Z_{\delta_s}}$	Change in C_Z due to δ_s change
C_{X_α}	Change in C_X due to α change
C_L	Coefficient of Lift (C_L = Lift/qS)
C_D	Coefficient of Drag (C_D = Drag/qS)
γ	Flight Path Angle
θ	Pitch Angle
V	Aircraft Velocity (Forward)
$\dot{V}$	Aircraft Acceleration (Forward)
W	Weight of Aircraft = Mg
F	Summation of Forces
$\dot{F}UEL/T$	Linear Approximation of the Relation of Fuel Flow to Thrust $\left(\frac{Slug/sec}{lb}\right)$

Subscript

i	Inertial or Earth Axis Reference
m	Measured or Air Mass Reference
SEL	Selected

1.0 INTRODUCTION

Determination of true aircraft angle-of-attack has been a subject of much investigation and development. Two fundamental approaches to handle the problem have evolved; direct measurement of the airflow past the aircraft and calculation by inference through the combination of signals from previously available on-board sensors.

Direct airstream angle-of-attack measurement has had a relatively poor history with respect to accuracy and reliability. A good accurate measurement requires that the transducer be located in the free airstream ahead of the aircraft which is not always possible, particularly in high performance aircraft. Transducers located on the fuselage suffer from local flow effects and require calibration to minimize position error.

The reliability problem associated with external transducers is twofold. First, it is subject to all the extreme environmental conditions encountered by the aircraft. Second, it is an appendage on the fuselage, which is subject to mishandling damage. As an example, in one unfortunate installation the vane made a very convenient step for the pilot.

The deficiencies of vanes and probes has led to the investigation of computed alpha by inference from internally mounted sensors.

Various techniques for calculating angle-of-attack by inference were studied by Sperry Flight Systems under U.S. Air Force Contract F33615-69-C-1178 and documented in technical report AFFDL-TR-69-93. Using this information, a program was proposed to implement and evaluate the most promising of these techniques by flight test. The results of the implementation and evaluation program are presented in this report.

A summary of the program, briefly outlining the computation technique selected, development of the equipment, the ground and flight evaluation programs and the results and conclusions of the program, is contained in Paragraph 2.0.

Documentation of the analysis and test results of the program, including data reduction from the actual flight test recording, is presented in Paragraph 3.0.

Detail schematic drawings, test specifications and aircraft wiring data submitted to AFFDL with progress reports during the course of the program were not duplicated in this report.

2.0 SUMMARY

The objectives of the program were to select a suitable means for calculating the aircraft angle-of-attack using on-board sensors, to design and fabricate an implementation of the technique selected and to evaluate it in actual flight test. The technique selected was to compute angle-of-attack from air data, aircraft acceleration and surface positions. The computation was implemented in an analog-type airborne computer and evaluated in a U.S. Air Force RF-4C aircraft.

2.1 Computation Technique

A multitude of equations can be solved to yield airframe angle-of-attack, but most of them can be eliminated when considering a practical mechanization. Included among such equations are those which require inertial quality hardware and systems involving higher than first order functions of alpha and beta.

The implementation proposed for this program involved a complement of two methods. The basic scheme was to mechanize the equation describing the forces on the aircraft in the Z-body axis direction.

$$A_Z = \frac{qS}{M}\left[C_Z\ (\alpha,\ \delta_F) + C_{Z_{\delta_s}}\ \delta_s\right] \qquad (1)$$

The best possibility of high-accuracy alpha computation under all conditions of flight including turbulence was offered by Equation (1). A difficulty with this equation is that aircraft mass must be continuously computed. The most practical way to compute mass is with the Z-force equation, but this equation cannot be used to compute both mass and angle-of-attack unless there is additional, independent information available. The needed information can be obtained from an alternate expression for angle-of-attack.

A simplified expression, derived from the equations describing the acceleration of the aircraft at the cg, was used.

$$A_X \cos \alpha_i - A_Z \sin \alpha_i = g \frac{\dot{h}_i}{V_i} + \dot{V}_i \qquad (2)$$

The only simplifications are those which result in dynamic errors, since this value of angle-of-attack must only be very accurate statically (i.e., during trimmed flight).

In the complementary method, Equation (1) is used to compute an angle-of-attack which, in turn, is used in Equation (2) to compute an aircraft mass. The aircraft mass is then heavily filtered and used in Equation (2) to compute a complemented angle-of-attack. This proposed implementation is illustrated in Figure 1.

In theory, the long-term solution of angle-of-attack was to be derived from the α_i computation, and the turbulence and dynamic errors were to be removed by the α_c computation. The proposed mechanization was a dc analog computation; the long chain of multipliers, dividers and non-linear functions was difficult to implement accurately. Therefore, the scheme was actually implemented as shown in Figure 2, using a feedback technique to minimize mechanization errors.

2.2 Computer Design

Analog techniques provided the most economical means to fabricate an angle-of-attack computer for flight evaluation. It was inherently compatible with the available on-board sensors and was still adaptable to the solution of implicit computation loops.

The angle-of-attack processor designed for this flight test program uses microcircuit operational amplifiers as the basic computation element and pulsewidth modulation for multiplication and division operations. It is a dc computation analog system packaged in a standard ARINC 1/2 ATR long rack with circuitry mounted on plug-in metal cards. Its accuracy is commensurate with the accuracy of the available data sensors and the accuracy of the flight test data measuring and recording equipment.

2.3 System Evaluation

2.3.1 Ground Test and Installation

The completed angle-of-attack processor was installed and evaluated in an aircraft ground-based simulator at Sperry Flight Systems in Phoenix, Arizona prior to delivery to the U.S. Air Force. These tests proved valuable, particularly in rate and integrator circuit dynamic testing, windshear sensitivity studies and sensitivity to air data noise. Only minor parameter changes were found necessary during the on-aircraft, ground-test phase.

The RF-4C aircraft modification and installation were performed by U.S. Air Force personnel. Sperry personnel assisted in installation ground testing. The pretests in the ground-based simulator were instrumental in assuring a relatively trouble-free installation into the flight test aircraft.

The installed complement of equipment is listed in Table I with the signal data and supplier. The alpha vane was installed on a boom ahead of the nose of the aircraft to independently measure angle-of-attack for comparison purposes. The estimated accuracy of the vane output (installed) is ±1/2 to ±1 degree.

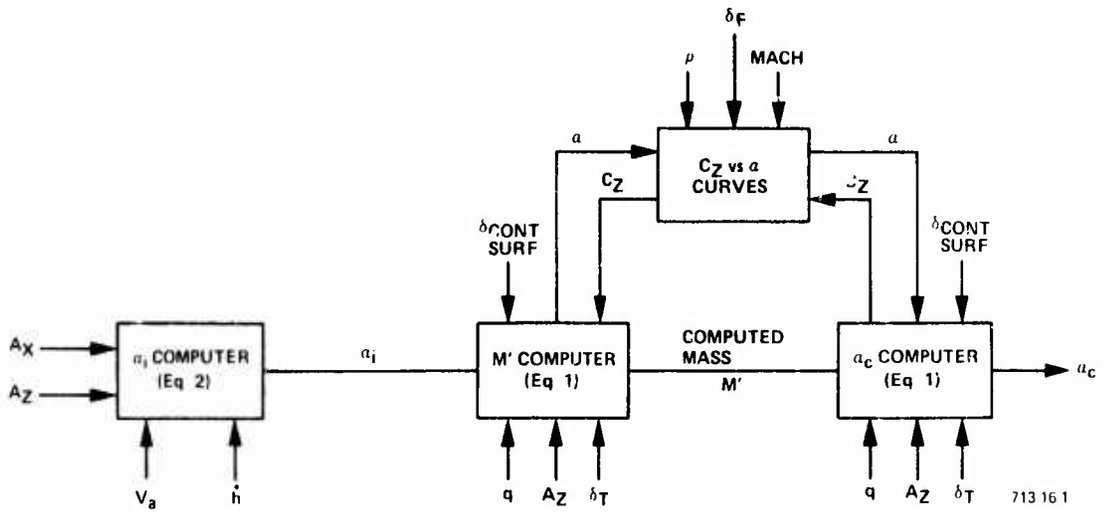

Figure 1
Simplified Block Diagram, Theoretical Implementation

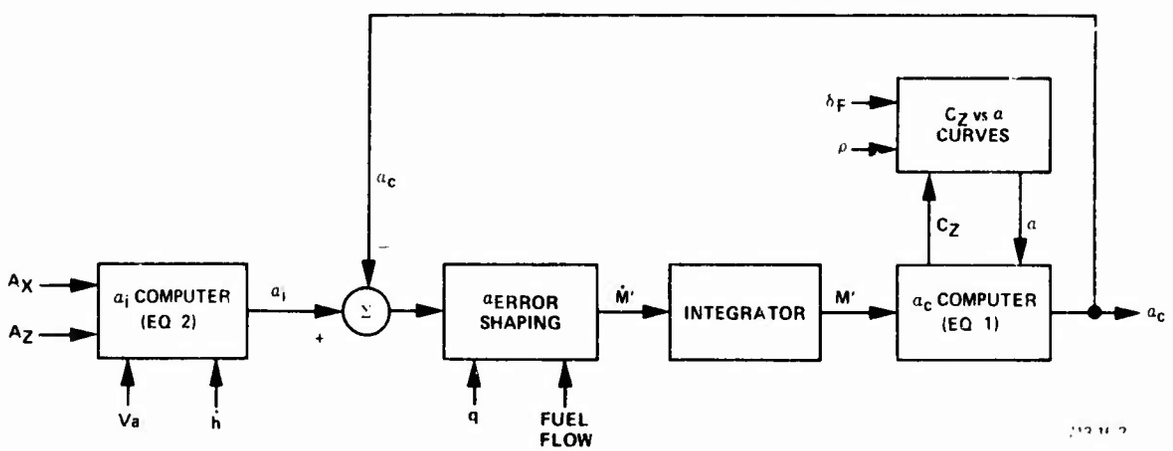

Figure 2
Simplified Block Diagram Final Implementation

TABLE I

INSTALLED COMPLEMENT OF EQUIPMENT

	Equipment	Sensed Quantity	Supplier
Normal RF-4C Complement	Inertial Nav Unit	Pitch Angle, Roll Angle, Vertical Velocity (θ, ϕ, $\dot{h}$)	USAF
	Central Air Data Computer	True Airspeed, Baro Altitude (V_a, h_B)	USAF
Additional Complement for Flight Test	Normal Accelerometer	Normal Accelerometer (A_Z)	USAF
	Longitudinal Accelerometer	Longitudinal Accelerometer (A_X)	USAF
	Lateral Accelerometer	Lateral Accelerometer (A_Y)	USAF
	Left Aileron Position Transducer Right Aileron Position Transducer	Aileron Position (δ_a)	USAF
	Stabilator Position Transducer	Stabilator Position (δ_s)	USAF
	Flap Position Transducer	Flap Position (δ_F)	USAF
	Lift Off Sensor Switch	On Ground/Off Ground	USAF
	Angle-of-Attack Vane	Measured Angle-of-Attack (α_m)	USAF
	Side-Slip Vane	Measured-Side Slip (β_m)	USAF
	Signal Conditioning Unit	---	USAF
	Flight Test Engineer Control Unit	---	USAF
	Tape Recording System	---	USAF
	Angle-of-Attack Processor	---	Sperry

2.3.2 Flight Tests

Computed angle-of-attack was evaluated under static and dynamic flight conditions. Static tests were conducted in straight and level flight for 3 minutes at each of seven constant airspeeds with flaps retracted and gear up, and at each of four airspeeds with flaps one-half extended and gear up. Dynamic tests were conducted at four airspeeds and altitudes with the following maneuvers:

- 1.8g pull-up to military power climb
- 0.2g pushover to idle power descent
- 180 degrees right followed by 180 degrees left turns pulling 1.8g
- +10 degrees side-slip followed by -10 degrees side-slip

2.3.3 Results and Conclusions

The results of the flight tests may be summarized as follows:

Test	Apparent Computed Alpha Error
Static Accuracy	
Flaps Retracted	Less than ±0.2 deg
One-half Flaps	Less than ±0.5 deg
Dynamic Accuracy	
Maneuvers	(1 deg max at 1/2 flaps) (0.5 deg max flap retracted)
Windshear (1 kt/sec)	No error
Side-slip (±10 deg)	No error

The apparent computed alpha error is referenced to the angle-of-attack measured by a vane and is, in reality, a relative error. The static errors listed included all system and recording tolerances. The dynamic errors demonstrate the true capability of this unique complementary technique and its potential in an integrated system design.

The computed angle-of-attack technique selected was demonstrated to be feasible and accurate with normally available, on-board sensors. Application of this technique to a specific aircraft and mission requirements would have to be studied and evaluated. Extremely high accuracy could be achieved over a wide range flight condition if accurate data sources are available and digital computation is employed. This technique is dependent on the slow computation of aircraft weight or mass and can only compute when the aircraft is flying.

3.0 PROGRAM DOCUMENTATION

3.1 System Design

3.1.1 Interface Data

A block diagram of the angle-of-attack computation system as installed in the RF-4C test aircraft (showing the interface with the on-board sensors and the final implementation of the processor) is illustrated in Figure 3. The detail design of the angle-of-attack processor was dictated, to some extent, by available input data in the test aircraft. Dynamic pressure (q) was not available from the central air data system. Therefore, true airspeed (V_a) and barometric altitude (h) were used to compute q based on standard atmospheric conditions.

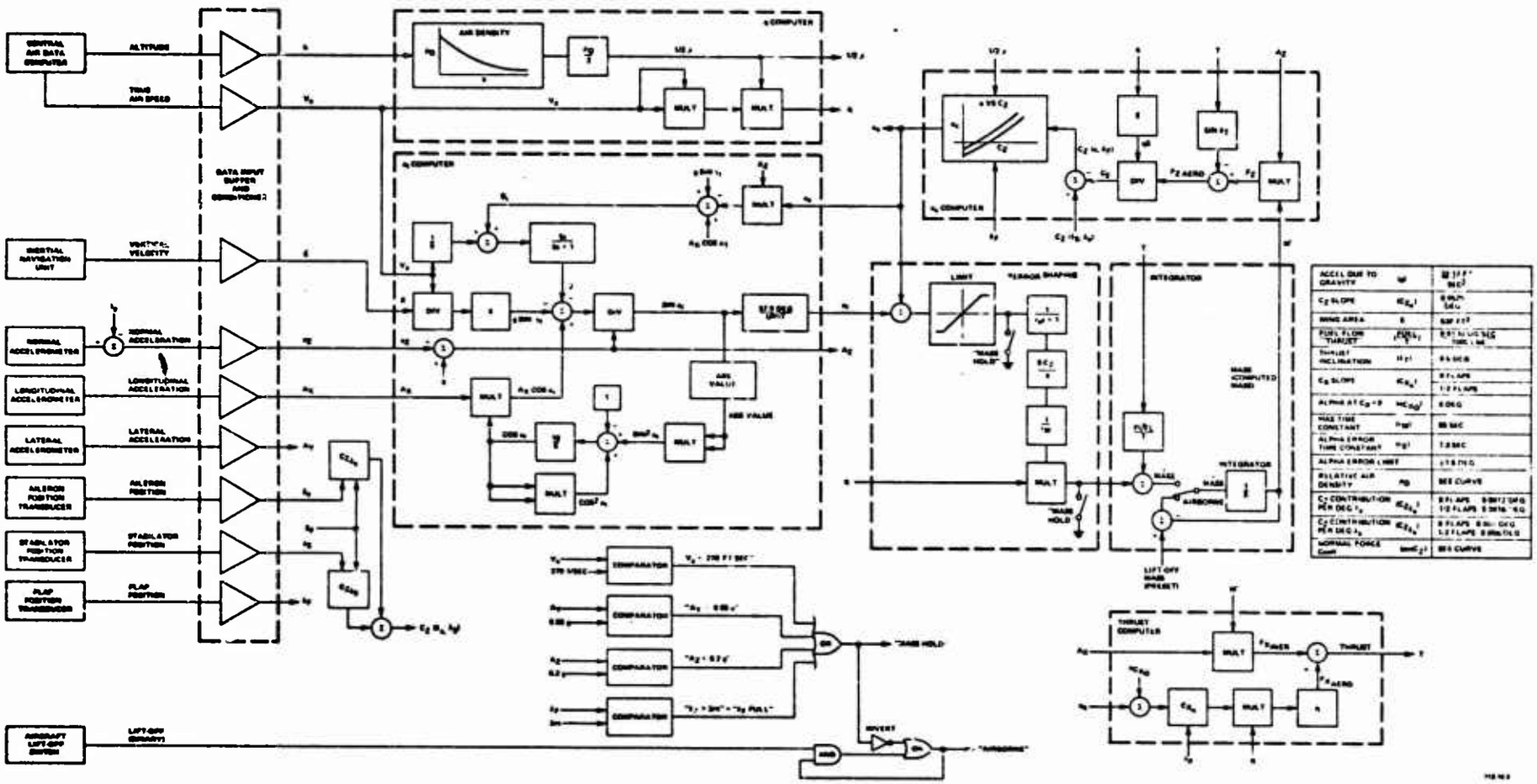

Figure 3
Angle-of-Attack Computation System
Block Diagram

Originally, it was proposed to derive thrust data from throttle position. Subsequent analysis indicated that thrust could be derived more easily and accurately from available data as shown in Figure 3.

3.1.2 System Limitations

The aircraft flight performance limitations for evaluation of the angle-of-attack computation system are listed in Table II. These limitations were dictated by analog computing techniques, input data and available aerodynamic data on the RF-4C aircraft. A lower limit of 150 knots for true airspeed from the central air data computer also limited flaps to one-half or up positions and landing gear in the up position.

TABLE II

FLIGHT PERFORMANCE LIMITATIONS

Normal Acceleration	0 to 2g
Longitudinal Acceleration	±1g
Mach	0.95
Thrust	Mil thrust max
Maximum "q"	667 lb/sq ft
Pitch and Roll Angles	0 ± 60 deg
Angle-of-Attack	-10 to +18 deg
Speed Brakes	Retracted
BLC	Operating
Gross Weight	50,000 lb max
Altitude	-1,000 to 50,000 ft

Without the limitations listed in Table II, the following aircraft data would have been required and stored as function generators in the analog angle-of-attack processor:

- Normal force coefficient (C_Z) as function of flaps, alpha, Mach, and air density
- Longitudinal force coefficient (C_X) as function of flaps, alpha, Mach and air density
- Change of normal force coefficient due to Δ stabilator ($C_{X_{\delta_s}}$) as function of flaps, Mach, alpha, and air density
- Change of normal force coefficient due to aileron/spoiler ($C_{Z_{\delta_a}}$) as function of Mach and air density

With the limitations imposed, it was possible to simplify these functions as follows:

- C_Z was made independent of Mach by limiting M to 0.95 maximum.
- C_X was also made independent of Mach, and linearized with respect to alpha at each of two flap positions.
- $C_{X_{\delta_s}}$ and $C_{Z_{\delta_a}}$ were made independent of Mach, and linearized with respect to surface movement at each of two flap positions.

The RF-4C data was supplied by AFFDL as lift (C_L) and drag (C_D) data which had to be resolved into the X and Z axis as follows:

$$C_Z = C_L \cos \alpha + C_D \sin \alpha$$

$$C_X = C_D \cos \alpha - C_L \sin \alpha$$

3.1.3 Error Shaping

The α_{error} shaping circuitry performs the function of establishing the level of control of α_i over α_c which it does by controlling open loop gain and the roll-off frequency of α_i control. It also attenuates high frequencies by further filtering the error signal and by limiting the error magnitude.

As stated in Paragraph 2.1, the computed α_i signal is accurate in constant speed wind, but is in error in changing wind. This suggests that the roll-off frequency for α_i should be based on expected windshear values. Study of available literature led us to a preliminary decision. If a simple lag response were used, a roll-off frequency of approximately 1/110 radians per second at low altitudes down to 1/440 radians per second at high altitudes would be required to hold error due to (moderate to heavy) turbulence below 0.2 degree. Error frequencies caused by flight perturbations were estimated to be well above those frequencies, leaving turbulence as the limiting factor. The 1/110 to 1/440 roll-off was built into the computer. In addition, another filter was specified to smooth the error signal and a limiter to limit the magnitude of error. The final setting of these three parameters was left to simulator evaluation and flight test.

The divide-by-q function, which is necessary in the α_c computer to calculate C_Z from F_Z, appears to work against the requirements for turbulence error attenuation. Since turbulence is essentially spatial in nature, the turbulence frequency seen by an aircraft is proportional to the speed with which it moves through the turbulent air. Therefore, the error roll-off frequency should probably be proportional to true airspeed. The division by q actually makes this roll-off frequency inversely proportional to true airspeed. Correction of this characteristic would require a multiply-by-q^2 function in the error shaping circuitry. In the absence of hard information that this function was really required, it was decided that a compromise multiply-by-q function would be employed. This causes the roll-off frequency to be independent of airspeed.

3.2 Analog F-4 Simulator Development

3.2.1 Simulator Purpose

Early in the program, it was planned that an analog simulation of the test aircraft would be generated, which could interface with the angle-of-attack processor hardware. With this interface, a ground evaluation of the computer system was planned prior to aircraft installation and flight test.

3.2.2 Simplification of Equations

It was obvious at the start that it was not necessary to duplicate the pitching, rolling, and yawing dynamics of the test aircraft. To evaluate the angle-of-attack processor, it would be necessary only to force attitude disturbances through as simple a means as possible.

Since data was not available, the effects of side-slip on lift and drag, simulator evaluation of the effects of lateral forces due to slip was not attempted.

It was also decided that nothing could be learned from simulation of aircraft turning maneuvers. Therefore, the required simulation was reduced to movements in the X-Z plane and simple pitch angle forcing of a point mass vehicle. However, the equations could not be linearized because of the large disturbances required.

3.2.3 Specifications

The following inputs were required:

- Elevator commands from a simple flight path angle select autopilot
- Throttle commands from a simple true airspeed select autothrottle
- Vertical and horizontal wind in the form of simulated turbulence of light, moderate and heavy intensity

The following outputs were required for interface with the angle-of-attack processor:

Longitudinal Accelerometer	A_X
Normal Accelerometer	A_Z
Vertical Rate	$\dot{h}$
Baro Altitude	h
True Airspeed	V_a
Stabilator Angle	δ_S
Flap Position	δ_F

3.2.4 Aircraft Equations

The large disturbance equations of motion implemented in the analog computer were developed from the following acceleration and force relationships as defined in Figures 4 and 5.

$$\dot{V}_i = a_x \cos \alpha_i - a_z \sin \alpha_i \tag{3}$$

$$\ddot{h}_i = a_x \sin \theta + a_z \cos \theta \tag{4}$$

$$f_z = W \cos \theta + T \sin \lambda_T + qS [C_Z] \tag{5}$$

$$f_x = T \cos \lambda_T - W \sin \theta - qS [C_X] \tag{6}$$

$$a_x = f_x/M \tag{7}$$

$$a_z = f_z/M \tag{8}$$

In terms of accelerometer outputs A_X and A_Z

$$a_x = A_X - g \sin \theta \tag{9}$$

$$a_z = A_Z - g \cos \theta \tag{10}$$

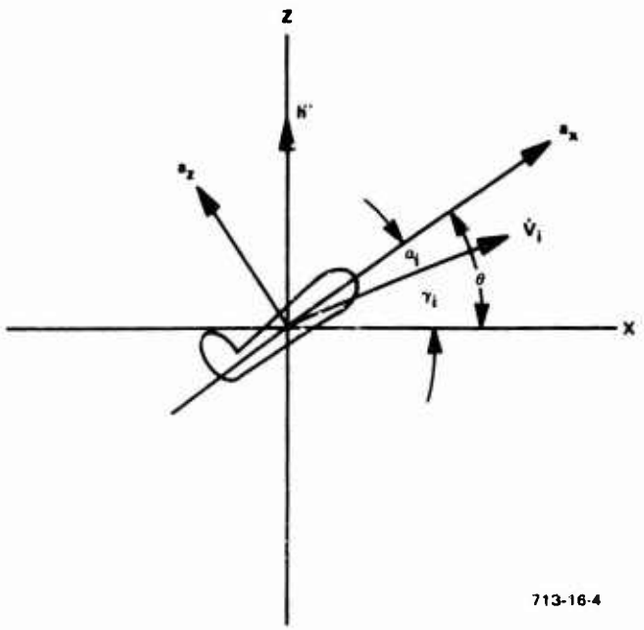

Figure 4
Aircraft Acceleration in Vertical Plane

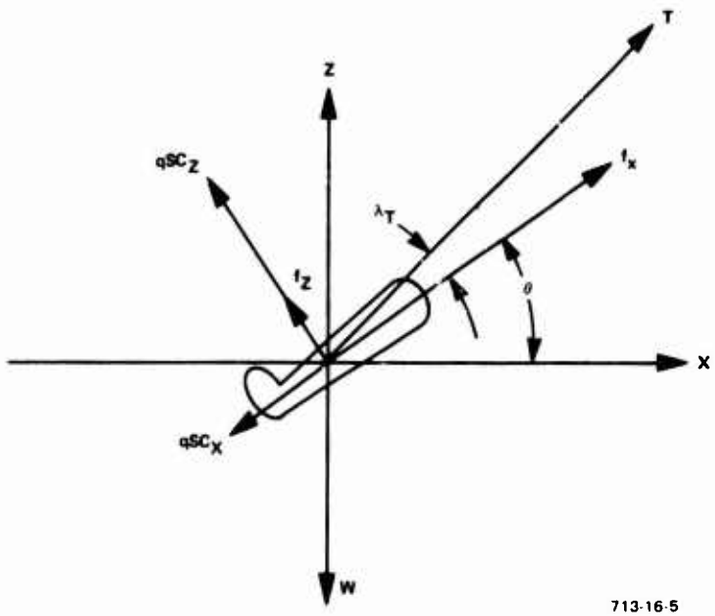

Figure 5
Aircraft Force in Vertical Plane

Substituting Equations (9) and (10) into Equations (3) and (4),

$$\dot{V}_i = A_X \cos \alpha_i - A_Z \sin \alpha_i - g \sin \gamma_i \tag{11}$$

$$\ddot{h}_i = A_X \sin \theta + A_Z \cos \theta - g \tag{12}$$

Dividing Equations (9) and (10) by M

$$f_x = F_X - W \sin \theta \tag{13}$$

$$f_z = F_Z - W \cos \theta \tag{14}$$

Substituting Equations (13) and (14) into Equations (5) and (6),

$$F_X = T \cos \lambda_T + qS [C_X] \tag{15}$$

$$F_Z = T \sin \lambda_T - qS [C_Z] \tag{16}$$

The aircraft motions then are described by the following equations which were programmed on an analog computer.

$$\dot{V}_i = A_X \cos \alpha_i - A_Z \sin \alpha_i - g \sin \gamma_i \tag{17}$$

$$\ddot{h}_i = A_X \sin \theta + A_Z \cos \theta - g \tag{18}$$

$$F_X = T \cos \lambda_T - qS [C_X] \tag{19}$$

$$F_Z = T \sin \lambda_T + qS [C_Z] \tag{20}$$

$$\sin \gamma_i = \dot{h}_i / V_i \tag{21}$$

$$\sin \gamma_m = \dot{h}_m / V_m \tag{22}$$

$$V_m = V_i + V_{wind_{horiz}} - V_{wind_{vert}} \sin \gamma_M \tag{23}$$

$$\dot{h}_m = \dot{h}_i + V_{wind_{vert}} \tag{24}$$

$$\alpha_i = \theta - \gamma_i \tag{25}$$

$$\alpha_m = \theta - \gamma_m \tag{26}$$

$$C_X = C_{X_\alpha} \alpha_M + C_{X_o} \tag{27}$$

$$C_Z = C_Z (\alpha_M, \delta_F)^* + C_{Z_{\delta_s}} \delta_s \tag{28}$$

---

*The C_Z versus α curves were programmed as exact duplicates of the angle-of-attack processor.

$$\theta = \theta_o + \delta_s \text{ K/s} \tag{29}$$

$$q = \frac{1}{2} \rho V_M^2 \tag{30}$$

$$W = W_o - \frac{\dot{FUEL}}{T} T \frac{1}{s} \tag{31}$$

$$M = \frac{W}{g} \tag{32}$$

$$A_X = \frac{F_X}{M} \tag{33}$$

$$A_Z = \frac{F_Z}{M} \tag{34}$$

$$a_z = A_Z - 1g \tag{35}$$

$$\rho = \frac{\rho}{\rho_o} \times \rho_o \tag{36}$$

where $\frac{\rho}{\rho_o} = f(h)$*

Autopilot Control Law

$$-\delta_s = \frac{1}{40} (\gamma_{SEL} - \gamma_i) - 4 \dot{\theta} \frac{1}{2s + 1}$$

Autothrottle Control Law

$$\Delta T = 200 \left[(V_{SEL} - V_M) + 200 \sin \gamma_M - (V_M - 6.2 \dot{V}_i) \frac{1}{10s} \right]$$

*The density ratio was programmed as the exact duplicate of the angle-of-attack processor.

3.2.5 Turbulence Simulation

The turbulence model is based on the power spectral technique. By this technique turbulence is described as a stationary random Gaussian process. The term "stationary" implies that the statistical properties of the process do not vary with time.

Considering first the longitudinal component of trubulence; in Reference 1, the longitudinal component of turbulence is assumed to be represented by a Gaussian process having a spectrum of the form:

$$\Phi(\Omega) = \sigma^2 \frac{2L}{\pi} \frac{1}{1 + \Omega^2 L^2} \tag{37}$$

where:

$\Phi(\Omega)$ =	power spectral density	$\frac{(ft/sec)^2}{rad/ft}$
σ =	standard deviation of wind velocity (rms turbulence intensity)	ft/sec
L =	turbulence scale factor	ft
Ω =	spatial frequency	rad/ft
ω =	time frequency = $V \cdot \Omega$	rad/sec
V =	velocity of aircraft relative to air mass	ft/sec

The power spectral density can be simulated by a white noise generator through an appropriate filter. Details of the derivation are presented here.

First, it is necessary to redefine the power spectral density in terms of radian time measure, that is $\Phi(\Omega)$ must be converted to $\Phi(\omega)$:

The power spectral density is defined such that

$$\int_0^\infty \Phi(\Omega)\, d\Omega = \sigma^2 \tag{38}$$

Substituting $\Omega = \frac{\omega}{V}$ into Equation (38),

$$\int_0^\infty \frac{\Phi(\Omega)}{V} d\omega = \int_0^\infty \Phi(\omega)\, d\omega$$

where:

$$\Phi(\omega) = \frac{\Phi(\Omega)}{V}$$

Substituting into Equation (37),

$$\frac{\Phi(\Omega)}{V} = \Phi(\omega) = \sigma^2 \frac{2}{\pi} \frac{L}{V} \frac{1}{1 + \omega^2 (L/V)^2}$$

Letting $\omega_o = V/L$,

$$\Phi(\omega) = \sigma^2 \frac{2}{\pi\omega_o} \frac{1}{1 + (\omega/\omega_o)^2} \tag{39}$$

With the power spectral density now defined in terms of radian-time measure, the proper simulation analog can be derived as follows:

$\Phi(\omega)$ can be defined as $\Phi(\omega) = \sigma^2 \left| H'(j\omega) \right|^2$

where $\left| H'(j\omega) \right|$ is the magnitude of $H'(j\omega)$.

$$\left| H'(j\omega) \right| = \sqrt{\frac{2}{\pi\omega_o \left[1 + (\omega/\omega_o)^2\right]}}$$

Using a white noise generator the output can be shaped with a filter $H(j\omega)$ to obtain

$$\sigma^2 \left| H'(j\omega) \right|^2 = \Phi(\omega)$$

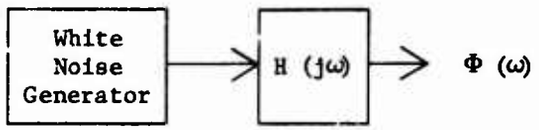

The power spectral density of the white noise generator is

$$\frac{RMS^2}{2\pi f_{BW}}$$

where:

RMS = rms value of white noise generator output voltage

f_{BW} = frequency bandwidth of white noise generator

Equating power spectral densities,

$$\frac{RMS^2}{2\pi f_{BW}} \times \left| H(j\omega) \right|^2 = \sigma^2 \left| H'(j\omega) \right|^2 \tag{40}$$

From this equation the desired filter H(S) may be derived (S = LaPlace operator).

Since σ is defined as an rms turbulence intensity, the rms value of the white noise generator can be set equal to σ.

$$RMS = \sigma$$

Canceling σ on both sides of Equation (40),

$$\frac{|H(j\omega)|^2}{2\pi f_{BW}} = |H'(j\omega)|^2 = \frac{2}{\pi\omega_o\left[1 + (\omega/\omega_o)^2\right]} \tag{41}$$

$H(j\omega)$ can be derived as follows:

$$|H(j\omega)|^2 = \frac{4\pi f_{BW}}{\pi\omega_o\left[1 + (\omega/\omega_o)^2\right]}$$

$$|H(j\omega)| = \sqrt{\frac{4 f_{BW}}{\omega_o\left[1 + (\omega/\omega_o)^2\right]}}$$

$$= \sqrt{H(j\omega)\, H(-j\omega)}$$

$$\therefore H(j\omega)\, H(-j\omega) = \frac{4 f_{BW}}{\omega_o\left[1 + (\omega/\omega_o)^2\right]}$$

and

$$H(j\omega) = 2\sqrt{\frac{f_{BW}}{\omega_o}}\,\frac{1}{1 + J\,\omega/\omega_o} \tag{42}$$

Letting $s = j\omega$ and substituting $V/L = \omega_o$ and $\omega_{BW} = 2\pi f_{BW}$

$$H(S) = 0.8\sqrt{\omega_{BW}\frac{L}{V}}\left(\frac{1}{\frac{L}{V}S + 1}\right) \tag{43}$$

The simulation of turbulence then becomes:

$$\Phi(\omega) = 0.8\,\sigma\sqrt{\omega_{BW}\frac{L}{V}}\left(\frac{1}{\frac{L}{V}S + 1}\right)$$

Magnitudes of σ and L are listed in Table III.

TABLE III

TURBULENCE SCALE FACTOR (L) AS A FUNCTION OF TURBULENCE INTENSITY (σ)

Altitude (ft)	White Noise Turbulence Intensity - (σ)		
	Light σ 7.5 ft/sec RMS (ft)	Moderate σ 15 ft/sec RMS (ft)	Heavy σ 30 ft/sec RMS (ft)
0 to 1,000	500	500	5,000
1,000 to 5,000	1,000	1,000	5,000
5,000 to 50,000	5,000	5,000	5,000

The white noise input was a tape with 0 to 35 Hz bandwidth and precalibrated to 0.3 volt RMS.

Although some of the literature defines a different distribution for vertical turbulence, Reference 1 assumes them to be identical. Sperry concurs that the simulation of the slightly different distribution function for vertical turbulence is not justifiable for our purposes. The minor differences would be overridden by assumptions and errors.

3.3 Angle-of-Attack Processor Design

The angle-of-attack processor designed for this program was adapted from a commercial computation system, which was in production at the time.

3.3.1 Hardware Design

A completely designed commercial electronics chassis was used in the F-4 aircraft (Figure 6). It was more than adequate in volume, allowing open, discrete component electronic circuit design techniques and the flexibility for probable flight test configuration modifications.

All parts were available from stock. There were no long-lead items to delay schedule and no spare parts problems for support of the test program. Sparsely populated metal plug-in circuitboards made testing and troubleshooting feasible without sophisticated test fixtures.

3.3.2 Circuit Design

Again, because of the concurrent production program, all circuits were previously designed and qualified to commercial specifications, which was entirely adequate for the flight test environment.

The dc analog circuitry used microcircuit operational amplifiers as the basic computation element and pulsewidth modulation for multiplication and division operations. For this single flight test computer, the required computational accuracy was achieved by the use of 0.1-percent resistors and by calibration. The dc computation allowed calibration using highly accurate digital voltmeters.

The analog computation techniques selected were also highly flexible to changes in aircraft parameters during the flight test program. Aircraft parameters were stored in the system in the form of function generators, which were easily adapted to flight test data collected during the system evaluation.

3.3.3 Test Fixture Design

The portable suitcase test fixture (Figure 7) was designed and constructed for use on the flight line and in the shop.

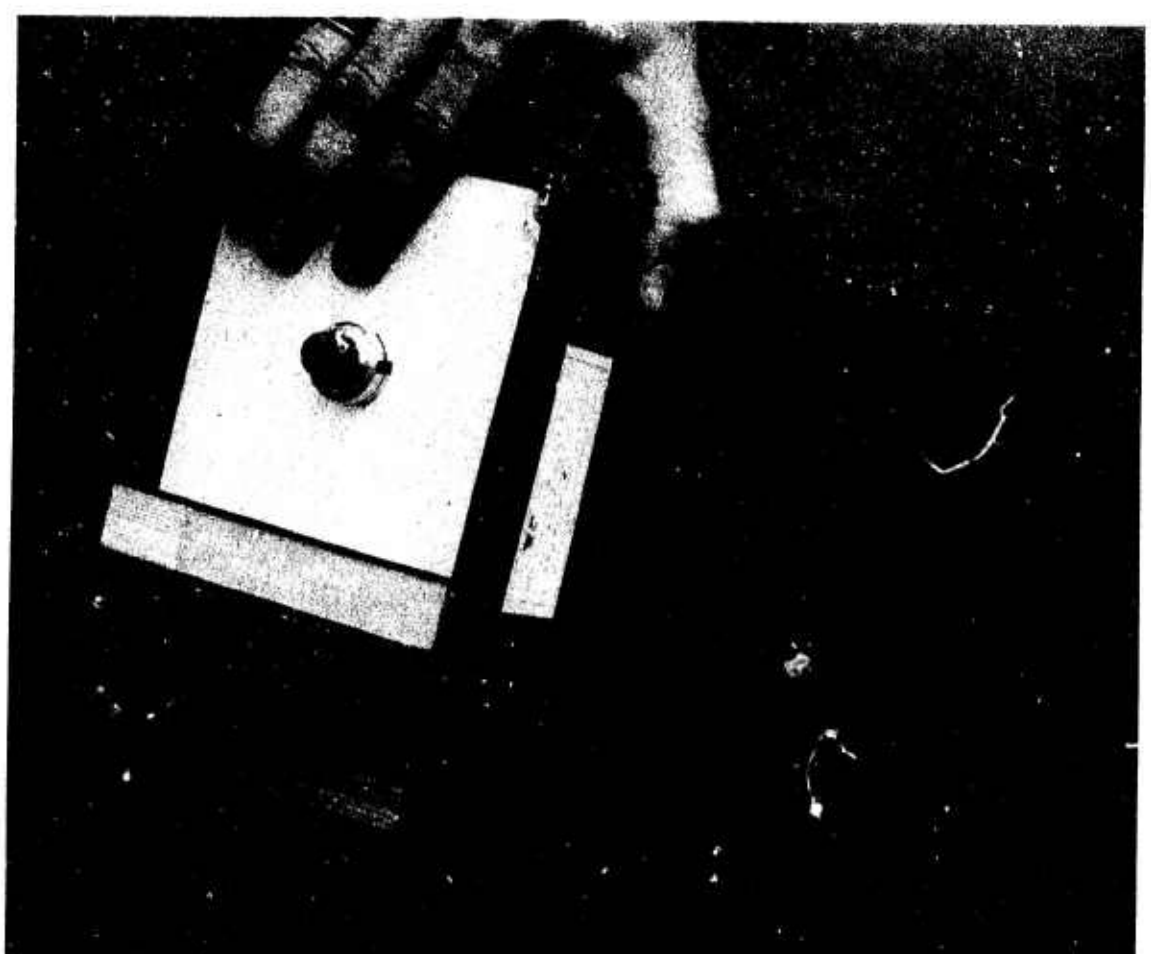

713-16-6

Figure 6
Angle-of-Attack Processor

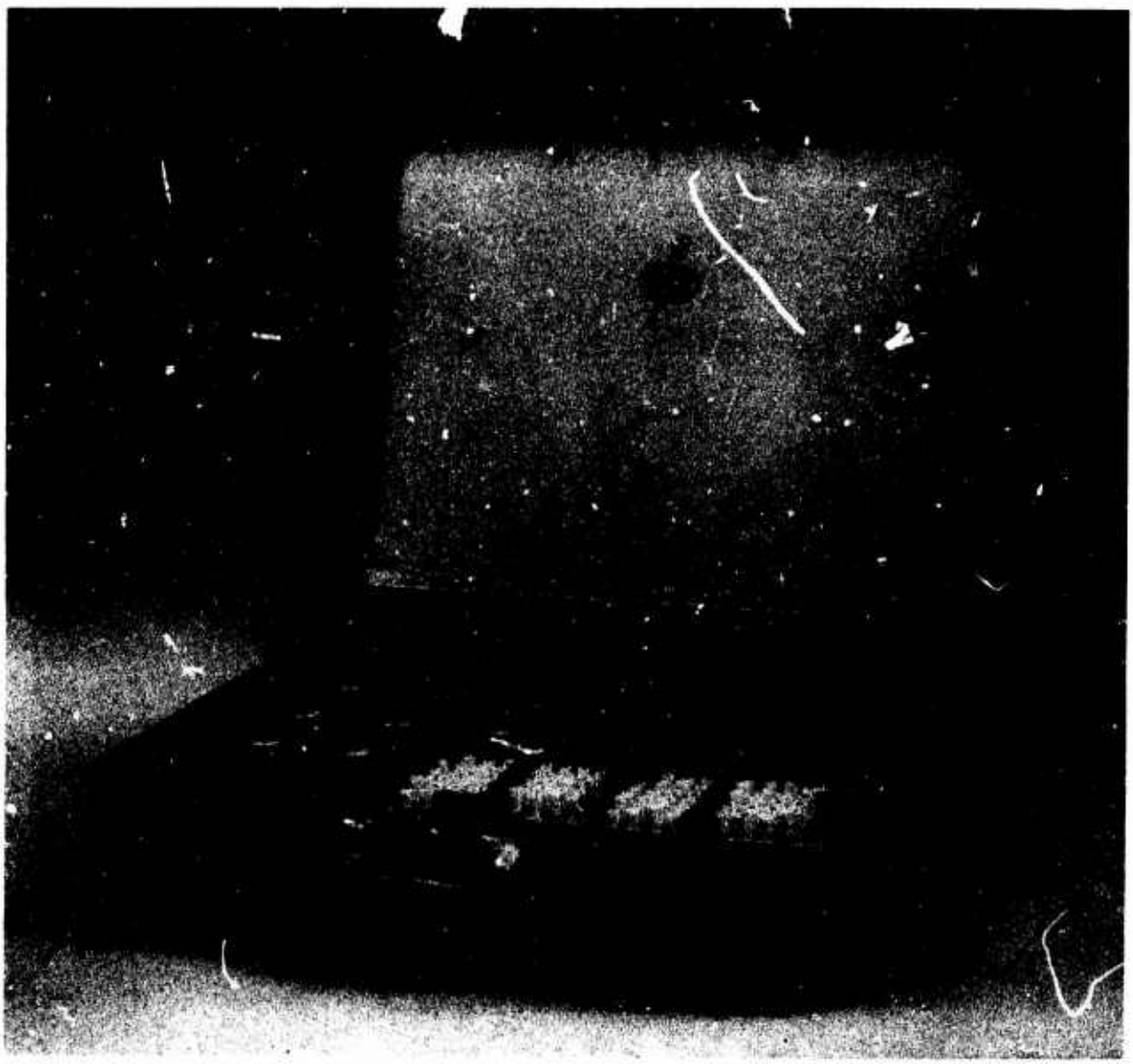

713-16-7

Figure 7
Suitcase Angle-of-Attack Processor Test Fixture

Design was simple, inexpensive and very flexible, necessary qualities in any prototype test equipment.

3.4 Ground Simulation Program

In the beginning of the program, the simulator test was thought of as an evaluation of the system preliminary to the flight evaluation. After progressing to the design of the simulator and then to the planning of the simulator test program, it became apparent that evaluation was not possible except in limited areas.

The computer was designed with published aircraft characteristics in memory. The same identical characteristics were also used in the simulated aircraft. Therefore, ground simulation could only validate implementation of the data. If could not evaluate the data relative to the real F-4 aircraft.

Simulator tests did have extensive value, however, in two other areas:

- As a dynamic functional bench test fixture
- In a limited preliminary evaluation of turbulence effects on computed alpha

3.4.1 Dynamic Test

With the aid of the simulator, it was possible to complete the bench testing of the computer. By programming such input problems as acceleration to a new speed and pullup and climb to a new altitude it was possible to monitor the portions of the computer which are responsive to changing conditions such as the true airspeed rate computer.

As a result of these tests, one unforeseen problem was made apparent. The airspeed rate taker was too noisy. The circuit was designed with a 1-second lag based on the assumption that the high frequency rejection designed into the dc computation would take care of the noise. It was apparent, however, that the magnitude of noise would drive amplifiers into the non-linear region and thereby cause standoff in α_i.

The problem was solved by increasing the $\dot{V}_a$ circuit lag to 5 seconds and compensating this lag with computed $\dot{V}_i$ (washed out). It is possible that the compensation or complimenting $\dot{V}_i$ is not required. It is dependent on the final selection of the α_i/α_c crossover frequency, which would not be firm until after flight test. The compensation was added to cover the possibility that a relatively high crossover frequency would be selected.

3.4.2 Turbulence Effects

The simulated aircraft and alpha computer system was subjected to the simulated turbulence, and the system performed qualitatively as designed.

A quantitative decision on the optimum crossover frequency was judged impossible, primarily because of the probable inaccuracy of the simulated turbulence. However, an adjustment was made in the crossover frequency based on an arbitrary limit of a ±1/4-degree alpha error due to moderate to heavy turbulence. It appeared that the original specification of 1/110 to 1/330 radian per second could be increased to 1/55 to 1/220 and still not exceed the limit.

The optimum crossover frequency is the highest possible while still limiting error to below the maximum permissible. It was decided that the final adjustment would have to be determined by flight test.

3.5 Test Aircraft Installation

3.5.1 Modification of the Test Aircraft

Installation requirements and interface data for the system shown in Figure 3 were supplied by Sperry, but modification of the RF-4C aircraft and actual installation of the

equipment was performed by U.S. Air Force personnel at Wright-Patterson Air Force Base. These tasks consisted of the following:

- Installation of the following equipment in the lower nose compartment in place of camera equipment

  Angle-of-Attack Processor with Mounting Tray

  Leach MTR 3200A FM Tape Recorder

  Air Force Designed and Constructed Signal Conditioner
  (serving primarily as isolation amplifiers for accelerometers)

- Installation of three orthogonally mounted accelerometers near the cg above the fuselage fuel cell No. 2, which supplied lateral, normal and longitudinal acceleration signals to the alpha processor

- Installation of surface position potentiometer transmitters on the flap, aileron (right), aileron (left), and stabilator which supplied electrical analog surface position signals to the angle-of-attack processor

- Installation of a nose mounted boom with vanes to measure and transmit electrical signals proportional to angle-of-attack and side-slip. (The angle-of-attack vane, although not required by the angle-of-attack processor, is required as an accurate reference against which the processor output can be compared. The side-slip vane supplies information for record, but is not required by the processor.)

- Installation of the flight test engineer's control panel

- Installation of all wiring interconnecting the above mentioned equipment as well as the air data system and inertial reference system

3.5.2 Ground Tests of Installed System

Ground tests were performed on the installed system to verify the interface of angle-of-attack processor and its signal input sources. Each signal transducer was physically moved a known amount, and the buffered input to the computer was monitored for correct gradient and zero reference.

Inertial Navigation System (INS) electrical pitch signal output was selected as the reference for angle-of-attack, and the accelerometers and the alpha vane were aligned with the INS platform. It was found during flight test that the INS zero was aligned approximately +3 degrees to the aircraft water line. Fortunately, this disagreement does nothing except shift the computed alpha and vane alpha about -3 degrees. All readings obtained in flight test are therefore about 3 degrees less than they would be if we had aligned with the aircraft waterline, which is the normal reference.

The ground tests were completed without major problems. Some trimming of signal gradients was required as expected. Recorder output gradients of the alpha computer had to be changed to be compatible with the recorder system. Two signal polarities had to be reversed. The accelerometer mounts had to be modified to allow for more accurate alignment.

3.6 Flight Test Program

The flight test program was conducted in two phases; Phase I consisted of shakedown and calibration flights, and Phase II included the record flights for final evaluation.

3.6.1 Phase I, Initial Flight Test

The first three flights were essentially shakedown flights which uncovered the following problems:

- Correction of processor/recorder interface problems
- Correction of the vane alpha (α_M) reference and gradient to track the inertial reference
- Assurance that all computed parameters were believable, and the recordings were accurate

After assurance that the system was performing correctly in a qualitative sense, a series of level constant speed runs were made to obtain data for confirmation of the stored normal force coefficient (C_Z) versus alpha (α_c) curves. Two flights were required.

This data was obtained based on the fact that $\theta_{INS} = \alpha_c$ in level constant speed flight. To maintain absolutely constant altitude and constant speed requires a good stable autopilot and calm air. The autopilot was unable to stabilize the aircraft at high angles-of-attack (above 7 to 8 degrees). Since the C_L curves are not straight above this level, the data could not be extrapolated. The accuracy, therefore, from 7 degrees upward was highly questionable. Each data run was taken at high gross weight (aft cg) and again at low weight (forward cg) to confirm the accuracy of the stabilizer lift program.

The C_Z versus α_c curves for aft cg and forward cg coincided and, therefore, it was concluded that stabilator lift calibration was correct.

The curves calculated from this experimental data are compared to those taken from the published F-4 aerodynamic data supplied by AFFDL in Figure 8. The curves agreed quite well in slope and shape, but the experimental curves were approximately -3 degrees displaced from the published curves. It was apparent at this point that the reference axis of the INS was not the same as the aircraft body axis. It was decided to stay with the INS reference axis. To change would have caused considerable delay with no real purpose.

The curves in processor memory were changed to reflect the new experimental data.

Four more flights (about 1.4 hours each) were required before the system was judged to be performing correctly for evaluation.

The Air Force had no way of accurately measuring the pressure input/voltage output characteristic of the INS vertical rate computation. Sperry, therefore, developed the following test to measure $\dot{h}$ error:

- Climb at 4000 feet per minute constant and 400 knots TAS
- Plot α_i versus α_M data for climb and descent
- Compare the α_i versus α_M data

Assuming no steady-state wind, the α_i and α_M data should be identical. If the climb data has higher α_i then the descent data, $\dot{h}$ gradient is low and vice versa. It is further assumed that TAS input has been verified to be accurate, which was the case. Data obtained by performing this test several times showed $\dot{h}$ gradient to be approximately 5 percent low.

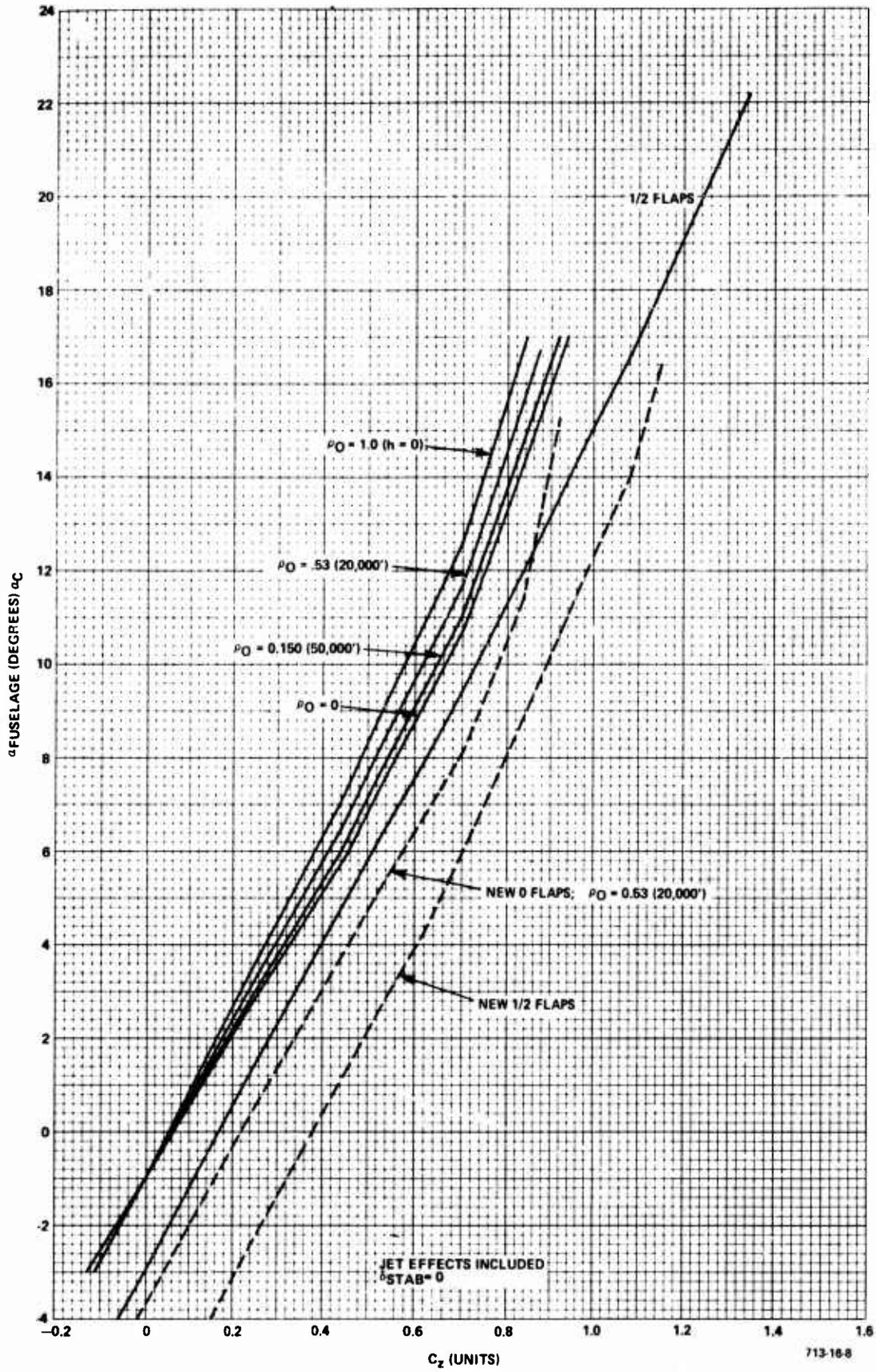

Figure 8
Comparison of C_Z and α_c

The $\dot{h}$ gradient was increased by 1.05 and the errors in climb and descent were considerably reduced in the following flights:

- Thrust Computation

  An error in the thrust computer was found during this period. It resulted from neglecting to resolve the inertial forces equation into the INS reference axis. A 3-degree bias added to the A_X input circuitry corrected the error.

- Vane Alpha and Computer Alpha Alignment

  The primary long-term reference for computed alpha in this system is the longitudinal accelerometer. Therefore, during installation the accelerometers were aligned with the INS pitch reference as accurately as possible. Since the mounts were not of production quality, the alignment was difficult and its accuracy questionable.

  The only measured alpha against which this system could be compared is the vane installed on a boom ahead of the nose of the aircraft. It was impossible to align this vane with the INS pitch reference accurately on the ground with the equipment available. Therefore, it was adjusted and readjusted after each of these flights based on recorded outputs during level flight runs. The target was exact tracking of INS pitch. Alignment results were much better than expected.

3.6.2 Phase II, Final Flight Tests

3.6.2.1 Flight Test Plan

Based on the flight performance limits listed in Table II, the following test plan was devised to assess the accuracy of the angle-of-attack computation system.

a. Static Tests

- Aircraft Configuration - 0 Flaps, Gear Up

  Straight/Level Flight, Constant Airspeed, 16,000 feet MSL

  3-minute run at CAS = Pedal Shake +20 knots (175 knots)
  3-minute run at CAS = 200 knots
  3-minute run at TAS = 300 knots
  3-minute run at TAS = 350 knots
  3-minute run at TAS = 400 knots
  3-minute run at TAS = 450 knots
  3-minute run at TAS = 500 knots

- Aircraft Configuration - 1/2 Flaps, Gear Up

  Straight/Level Flight, Constant Airspeed, 4,000 feet MSL

  3-minute run at CAS = Pedal Shake +10 knots (155 knots)
  3-minute run at CAS = Pedal Shake +20 knots (165 knots)
  3-minute run at CAS = Pedal Shake +35 knots (180 knots)
  3-minute run at CAS = 200 knots

b. Dynamic Tests

- Aircraft Configuration - 1/2 Flaps, Gear Up, 2,000 to 6,000 Feet

  Beginning at 2,000 feet MSL and 190 knots IAS

  1.8g pull-up to mil power climb at 190 knots

  Hold 190 knots at mil power to 6,000 feet

  0.2g pushover to idle power descent

  Hold 190 knots at idle power to 2,000 feet

  Pull-up and climb to 4,000 feet at 190 knots

  Hold 4,000 feet straight and level at 190 knots

  Make 180-degree right turn pulling 1.8g

  Make 180-degree left turn pulling 1.8g

  Induce 10-degree right side-slip for 10 seconds, then left side-slip holding level flight

- Aircraft Configuration - 0 Flaps, Gear Up, 5 to 15,000 Feet

  Beginning at 5,000 feet MSL and 220 knots IAS

  1.8g pull-up to mil power climb at 220 knots

  Hold 220 knots at full mil power to 15,000 feet

  0.2g pushover to idle power descent at 220 knots

  Hold 220 knots at idle power to 10,000 feet

  Pull-up to level flight and 220 knots at 10,000 feet

  Make 180-degree right turn pulling 1.8g

  Make 180-degree left turn pulling 1.8g

  From level flight at 220 knots induce 10-degree left side-slip, then 10-degree right side-slip holding level flight

  Level flight and accelerate at mil power (220 to 370 knots CAS) 15,000 feet MSL. Decelerate at idle power to 220 knots

- Aircraft Configuration - 0 Flaps, Gear Up, 15,000 to 25,000 Feet MSL

  Beginning at 15,000 feet and 350 knots CAS

  1.8g pull-up to mil power climb at 350 knots

  Hold 350 knots to 25,000 feet

  0.2g pushover to idle power descent at 350 knots

  Hold 350 knots to 20,000 feet. Pull-up to level flight at 20,000 feet and 350 knots.

  Make 180-degree right turn pulling 1.8g

  Make 180-degree left turn pulling 1.8g

  Induce 10-degree right side-slip for 10 seconds, then left side-slip for 10 seconds

- Aircraft Configuration - 0 Flaps, Gear Up, 25,000 to 35,000 Feet MSL

  Beginning at 25,000 feet and Mach - 0.75

  1.8g pull-up to mil power climb at 0.75M

  Hold 0.75M to 35,000 feet

  0.2g pushover to idle power descent at 0.75M

  Hold 0.75M to 30,000 feet. Pull-up to level flight at 0.75M

  Make 180-degree right turn pulling 1.8g

  Make 180-degree left turn pulling 1.8g

  Induce 10-degree right side-slip for 10 seconds, then left side-slip for 10 seconds

3.6.2.2 Flight Test Execution

a. First Attempt

The flight plan was executed on flights 10 and 11 (30 and 31 August). At first observation, the recorded data appeared to be satisfactory and was subjected to complete analysis. The detailed analysis uncovered errors. The thrust computer had failed causing 1/2- to 3/4- degree error upon change from full mil thrust to idle thrust.

A 2g pull-up resulted in an alpha near rudder shake and caused short term error of 1 to 1-1/2 degrees in α_c. Incorrect Z-force coefficient program in the high-alpha area was judged to be the cause. As mentioned previously, the accuracy in this region was considered questionable because the autopilot was unable to stabilize the aircraft for data runs. The 2g maneuver, however, allowed calculation of the C_Z error at high alpha, and stored data was corrected.

The thrust computer was repaired, and the C_Z versus α program was modified. Results of subsequent shakedown flights were satisfactory.

b. Second Attempt

The flight evaluation tests were rescheduled, but aircraft breakdowns and failure of the angle-of-attack vane caused extensive delays. On the second attempt (mid-November 1972) to complete evaluation flights all systems functioned, but the 1/2-flap, 190-knot dynamic test could not be made because of poor weather at 2,000 to 6,500 feet.

In addition, incorrect flight procedure resulted in an apparent 1-degree error at the beginning of the 220-knot dynamic test. In descending from 30,000 to 5,000 feet for the beginning of the 220-knot test, the pilot deployed speed brakes, which were not programmed into the stored aero data. Error built up to 1 degree during the descent and did not completely washout until well into the 180-degree turn maneuver. This can be seen in the $\alpha_c - \alpha_M$ trace (Figure 22). It was decided that this data was otherwise acceptable, and the discrepancy would be noted in the report and explained.

Just prior to these mid-November evaluation flights, the pitot/static system was determined by Air Force personnel to be incorrectly installed. This error was rectified by installing new pitot tubes on the correct sides of the aircraft and at the correct incident angles. The effects on the validity of the initial data where aircraft characteristics were calculated are unknown, but could be significant.

c. Third Attempt

The 1/2-flap, 190-knot dynamic test was rescheduled again and again, but further aircraft breakdowns delayed this run until mid-February.

During the 3-month delay, the true airspeed output of the central air data system decayed in quality to the level where it is of doubtful utility. Noise in the form of discontinuities due to a worn or dirty potentiometer can be easily seen on the true airspeed trace (V_a) (Figure 21). Steps of 25 feet per second and spikes of 75 feet per second are observed. Since this is internal noise and has no correlation with air movement, it causes significant errors (1- to 2-degree steps) and (up to 4-degree spikes) in computed alpha (α_c). If this type noise were caused by turbulence, the computer would not see any errors because the air movements would cause corresponding changes in lift and drag. In addition, during that delay, the alpha vane potentiometer opened and had to be disassembled and repaired. The reinstallation and realignment process resulted in a -1-1/2 degree shift in α_M.

3.7 Flight Test Evaluation Data

3.7.1 Static Tests

The results of the static tests are summarized in Table IV. With flaps retracted, computed and measured alpha agreed within 0.1 to 0.2 degree. With flaps at 1/2 extended, the errors were variable with an average of ±0.2 degree and a maximum of 0.3-degree variations.

Strip charts of each test run are included as Figures 9 through 19. Note that the resolution of the α_M sensor is quite poor (Figure 20). It is a wire-wound potentiometer and steps of 0.3 degree are apparent in the α_M and $\alpha_c - \alpha_M$ data.

In addition, the potentiometer is driven from the vane at a 1/1 ratio. If it is linear to 0.1 percent full scale (which is doubtful), another 0.3-degree error in α_M is possible.

In addition, the potentiometer is excited by + and - 15 volts with a virtual ground at center. There is no center tap so the electrical zero can drift with temperature and with power supply inequality. A 30-millivolt drift of one power supply would cause a shift of electrical zero of another 0.2 degree.

It must be concluded that the alpha vane cannot be considered to be an absolute measurement of angle-of-attack and that reference of computed to measured angle of attack in this report is relative, not absolute.

Error spikes of 1 to 2 degrees at 165 and 155 knots in the 1/2 flap configuration (Figures 18 and 19) are judged to be caused by discontinuities in the true airspeed transmitter potentiometer. This potentiometer appears to be noisest at low speeds. In this case, the extreme of the low range is specified as 150 knots true so these tests are very near that lower limit. Airspeed noise is discussed in more detail in paragraph 3.6.2.2.c.

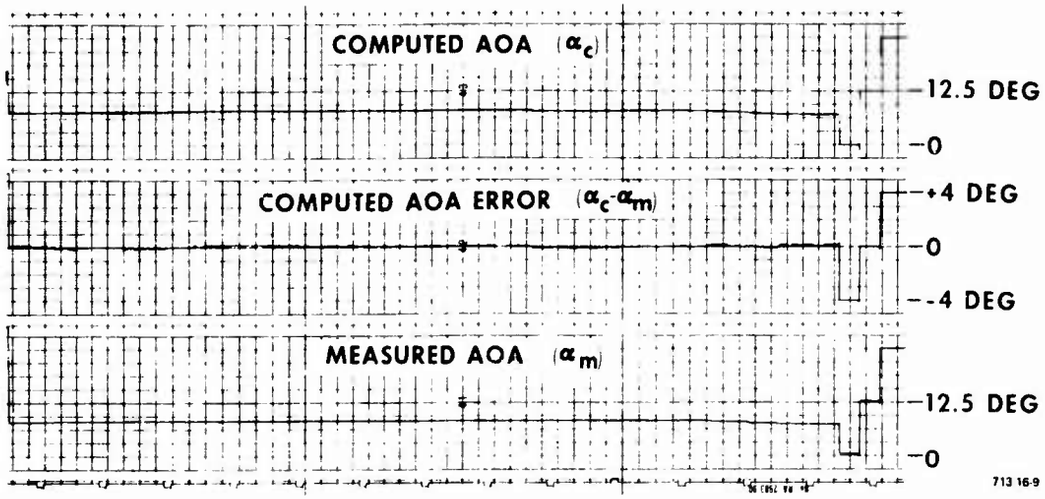

Figure 9
Static Evaluation, Flaps Retracted, α_M = 7.8 degrees, V_{CAS} = 178 knots

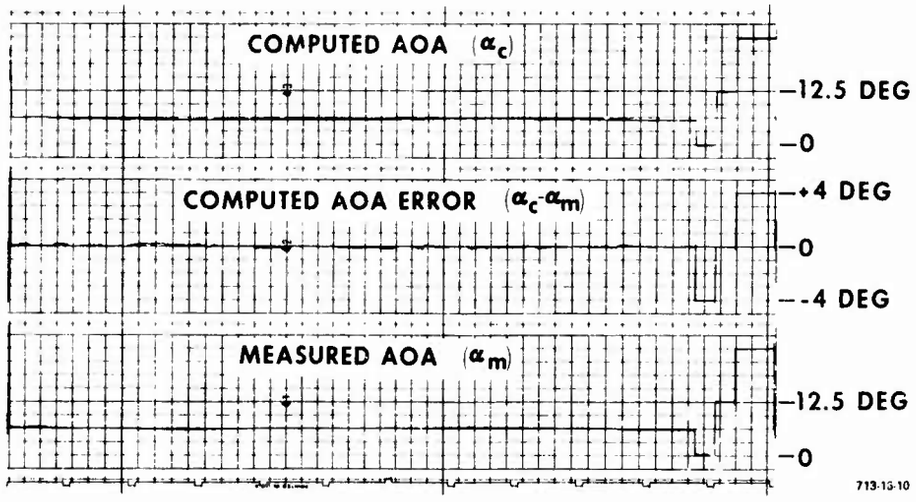

Figure 10
Static Evaluation, Flaps Retracted, α_M = 5.9 degrees, V_{CAS} = 201 knots

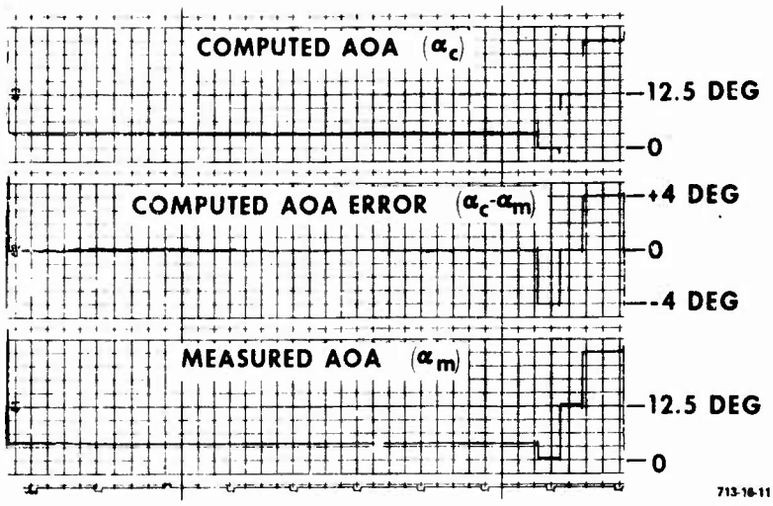

Figure 11
Static Evaluation, Flaps Retracted, α_M = 3.4 degrees, V_{TAS} = 299 knots

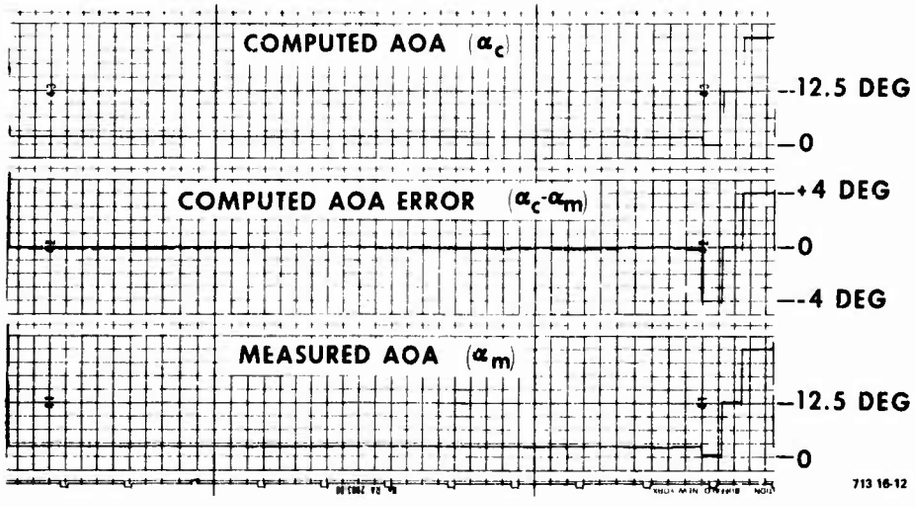

Figure 12
Static Evaluation, Flaps Retracted, α_M = 1.9 degrees, V_{TAS} = 348 knots

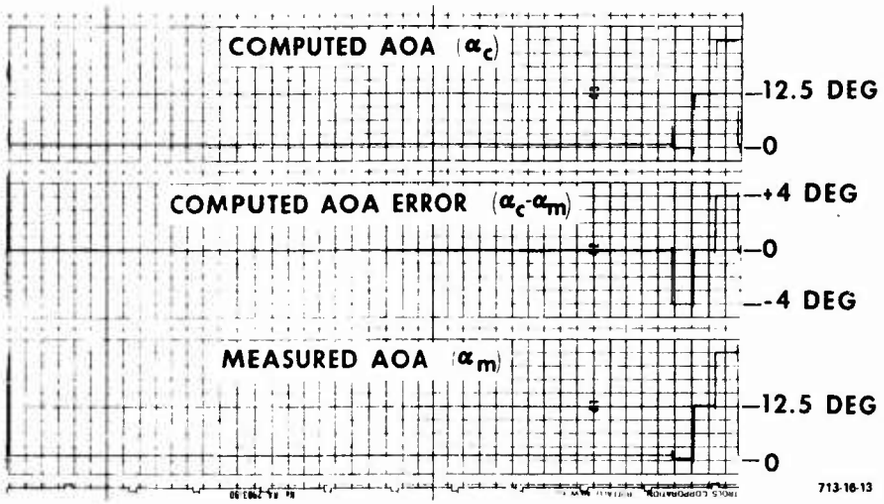

Figure 13
Static Evaluation, Flaps Retracted, α_M = 0.8 degree, V_{TAS} = 399 knots

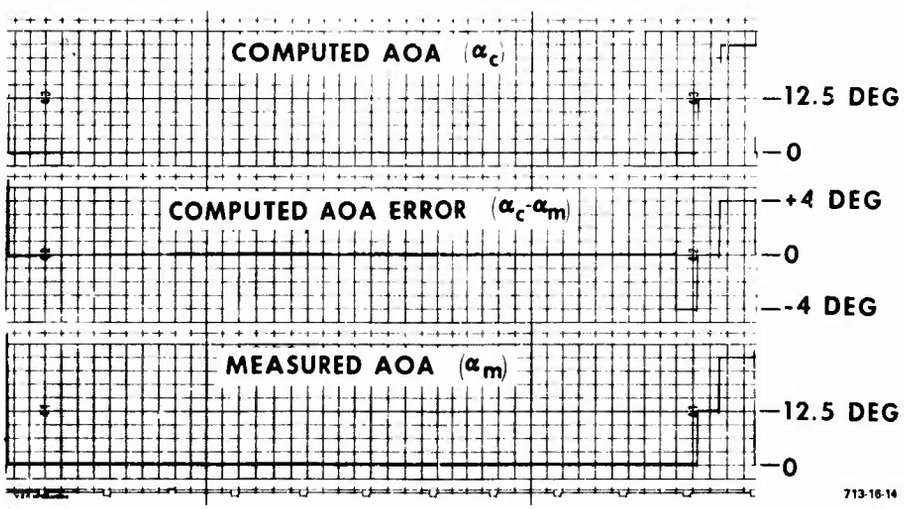

Figure 14
Static Evaluation, Flaps Retracted, α_M = 0.0 degree, V_{TAS} = 449 knots

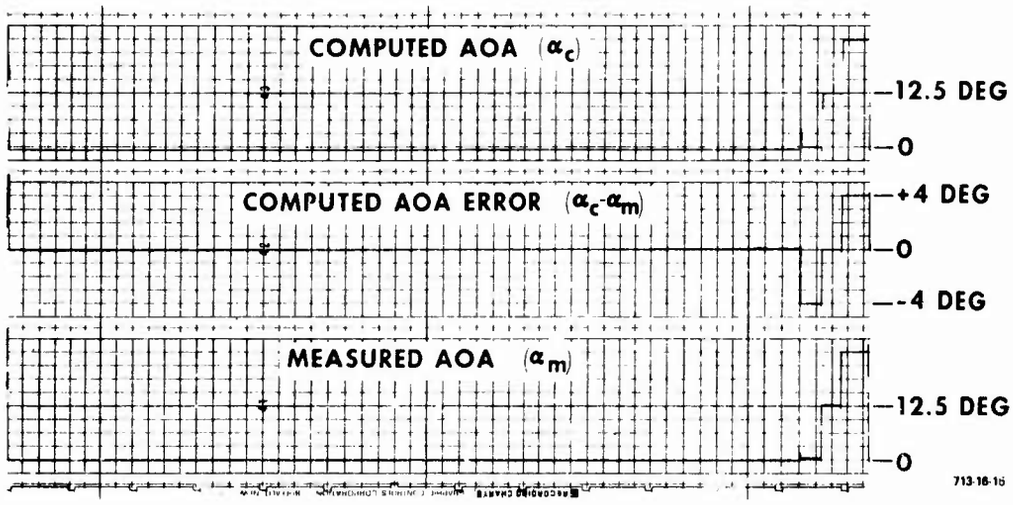

Figure 15
Static Evaluation, Flaps Retracted, α_M = -0.6 degree, V_{TAS} = 502 knots

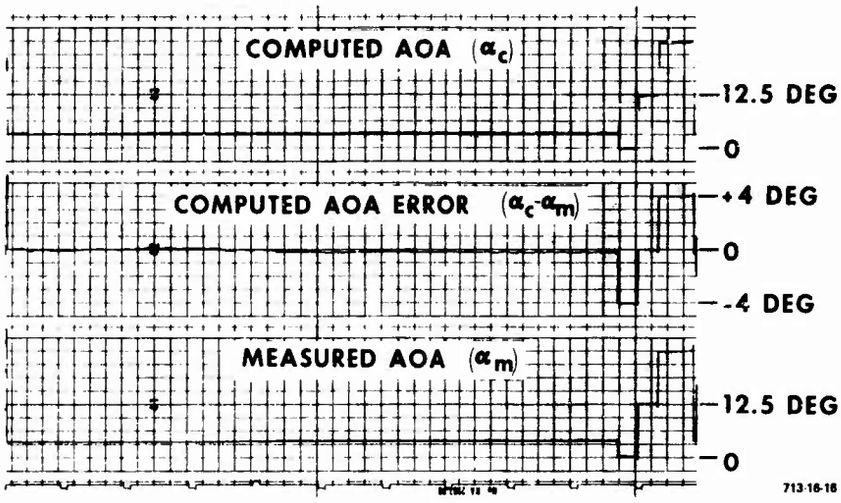

Figure 16
Static Evaluation, Gear Up/1/2 Flaps, α_M = 3.8 degrees, V_{CAS} = 200 knots

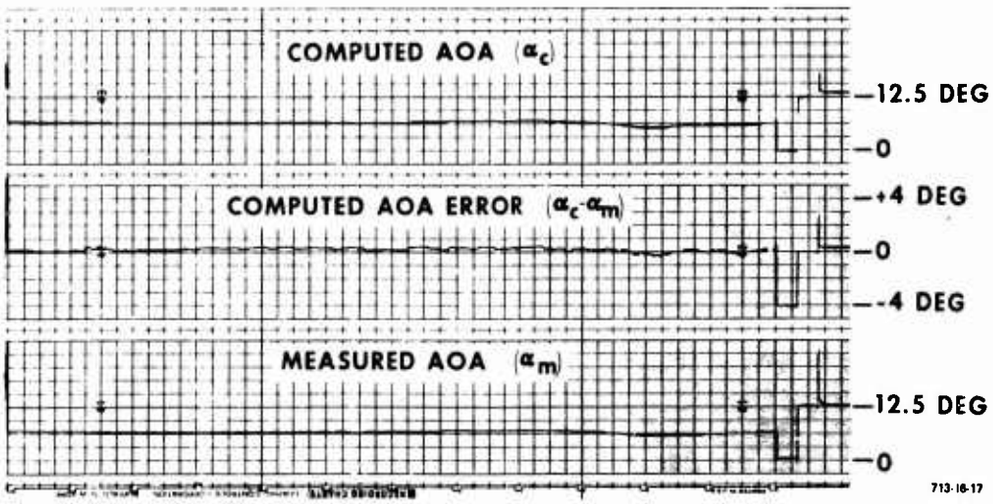

Figure 17
Static Evaluation, Gear Up/1/2 Flaps, α_M = 6.2 degrees, V_{CAS} = 178 knots

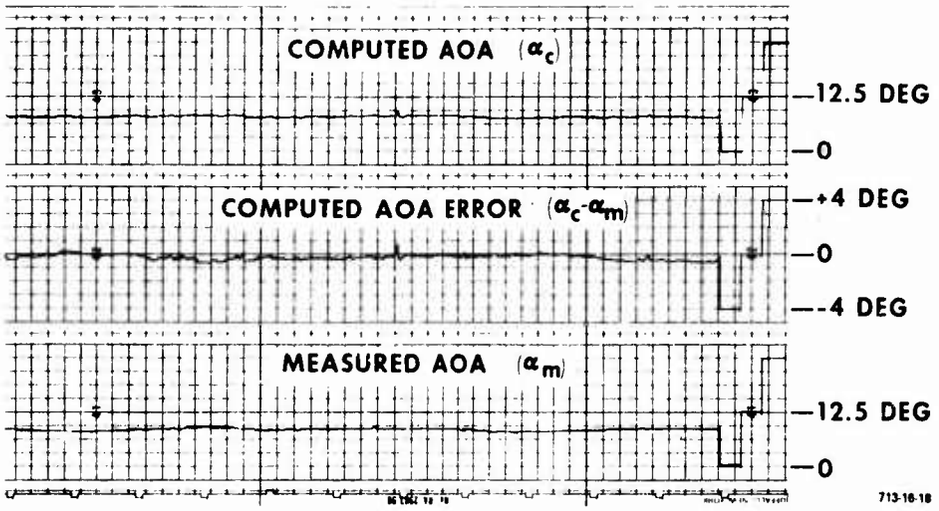

Figure 18
Static Evaluation, Gear Up/1/2 Flaps, α_M = 8.4 degrees, V_{CAS} = 165 knots

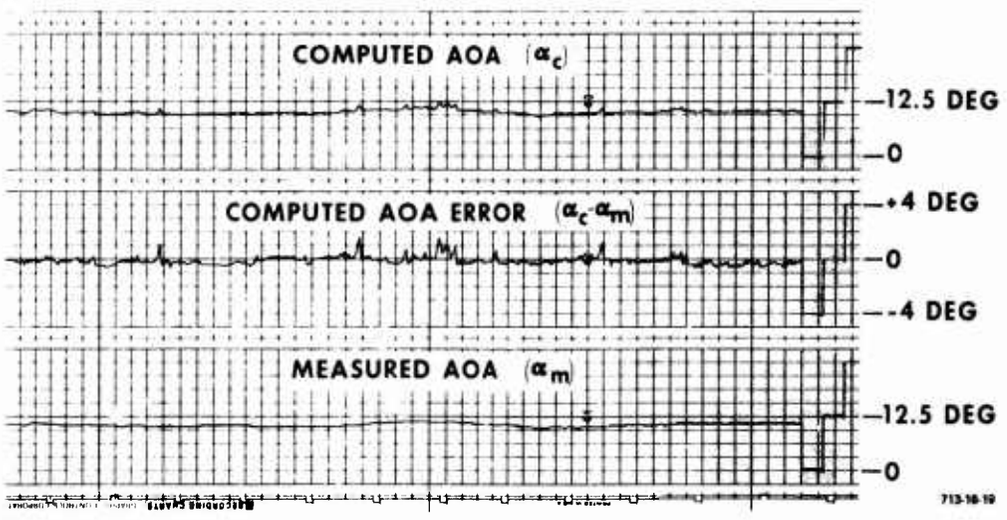

Figure 19
Static Evaluation, Gear Up/1/2 Flaps, α_M = 10.3 degrees, V_{CAS} = 155 knots

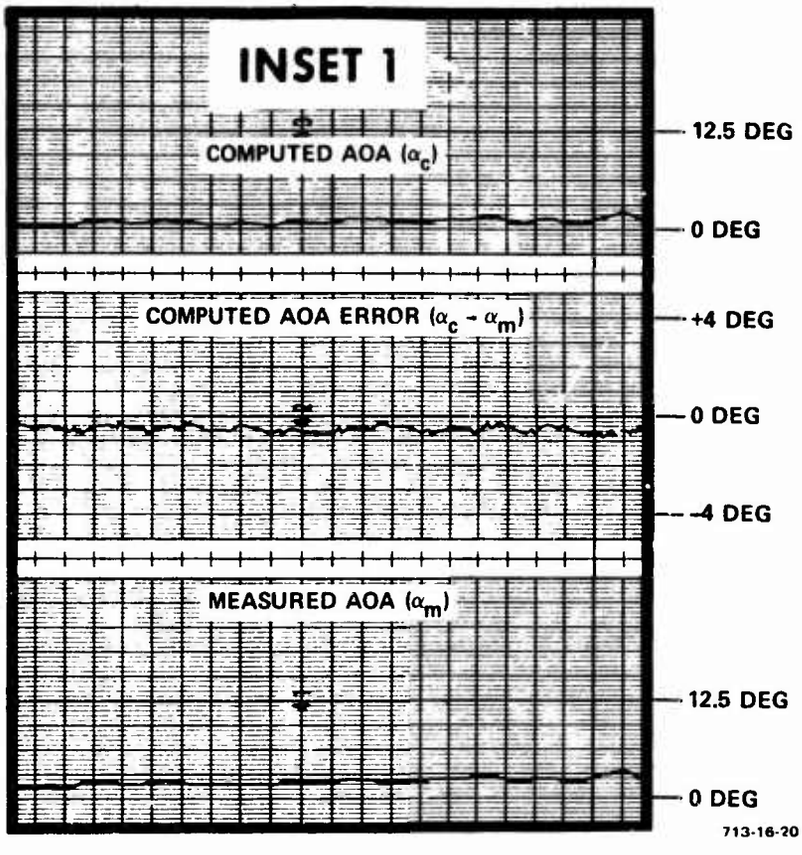

Figure 20
Vane Resolution
(Inset 1 of Figure 24)

TABLE IV

SUMMARY OF COMPUTED ALPHA STATIC ERRORS RELATIVE TO MEASURED (VANE) ALPHA

Airspeed	Flap Setting	Angle-of-Attack (deg)	$\alpha_c - \alpha_M$	Figure No.
178 CAS	Retracted	7.8	0.0 ± 0.1	9
201 CAS	Retracted	5.9	0.0 ± 0.2	10
299 TAS	Retracted	3.4	0.0 ± 0.1	11
348 TAS	Retracted	1.9	0.0 ± 0.1	12
399 TAS	Retracted	0.80	0.0 ± 0.1	13
449 TAS	Retracted	0.00	0.0 ± 0.1	14
502 TAS	Retracted	-0.6	0.0 ± 0.1	15
200 CAS	1/2 Flaps	3.8	-0.05 ± 0.15	16
178 CAS	1/2 Flaps	6.2	0.10 ± 0.25	17
165 CAS	1/2 Flaps	8.4	-0.25 ± 0.25*	18
155 CAS	1/2 Flaps	10.3	-0.2 ± 0.3*	19

*+1-degree noise spikes excluded

3.7.2 Dynamic Tests

The dynamic test results are illustrated in Figures 21 through 25.

3.7.2.1 Absolute Accuracy

With the exception of α errors caused by TAS noise, speed brake deployment and alpha vane alignment discussed in Paragraph 3.6.2.2, test results show that the relative angle-of-attack error ($\alpha_c - \alpha_M$) did not exceed 1 degree. In fact, most of the time the relative error was well within 1/2 degree. As mentioned previously, the accuracy, or more properly the inaccuracy, of the reference angle-of-attack as measured (Figure 20) by the vane together with the unknown accuracies of air data and the unknown effects of the pitot system change makes it impossible to assess the absolute accuracy of the angle-of-attack processor. Therefore, the demonstrated static accuracy must be regarded as acceptable.

3.7.2.2 Accuracy Under Disturbed Conditions

On the other hand, the accuracy of response to disturbances can be more precisely evaluated, possibly, to within ±1/2 degree error.

a. 1.7g to 2.0g Pull-Up Maneuver

At high speeds, error caused by this maneuver is not discernible. At low airspeeds, however, the effect of friction in the alpha vane and other errors begin to appear.

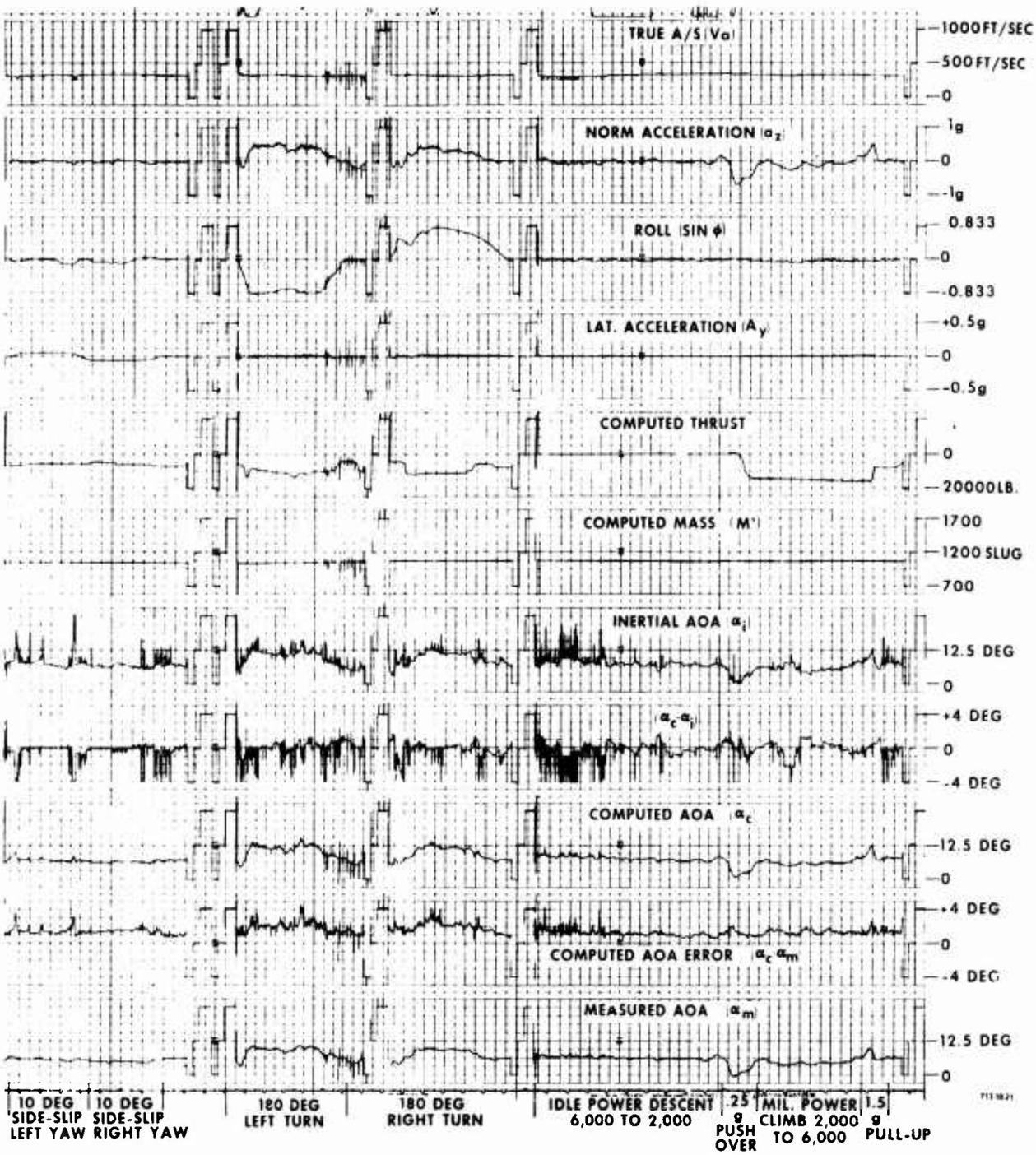

Figure 21
Dynamic Evaluation, 1/2 Flaps - 190 knots

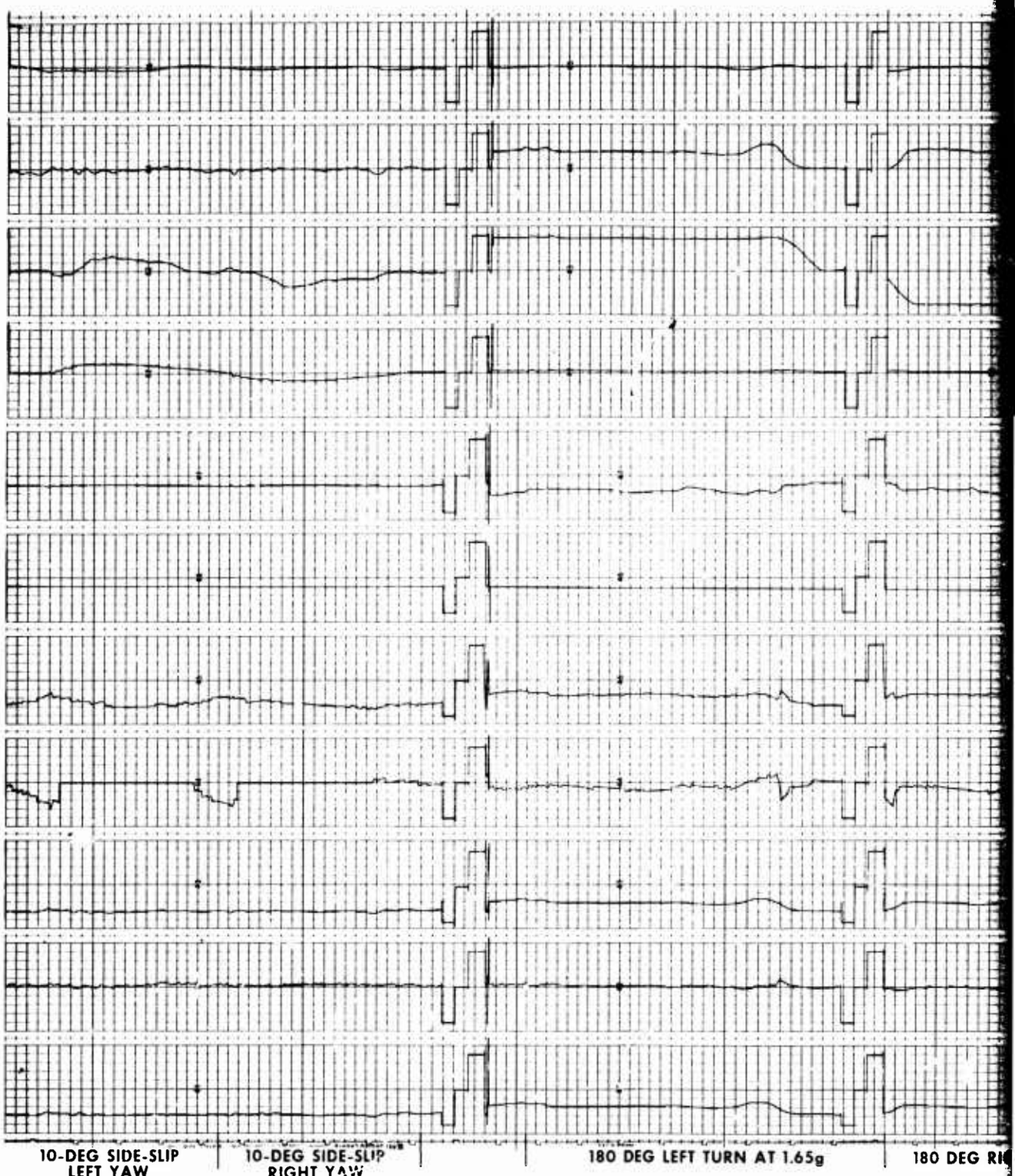
10-DEG SIDE-SLIP
LEFT YAW
10-DEG SIDE-SLIP
RIGHT YAW
180 DEG LEFT TURN AT 1.65g
180 DEG RI

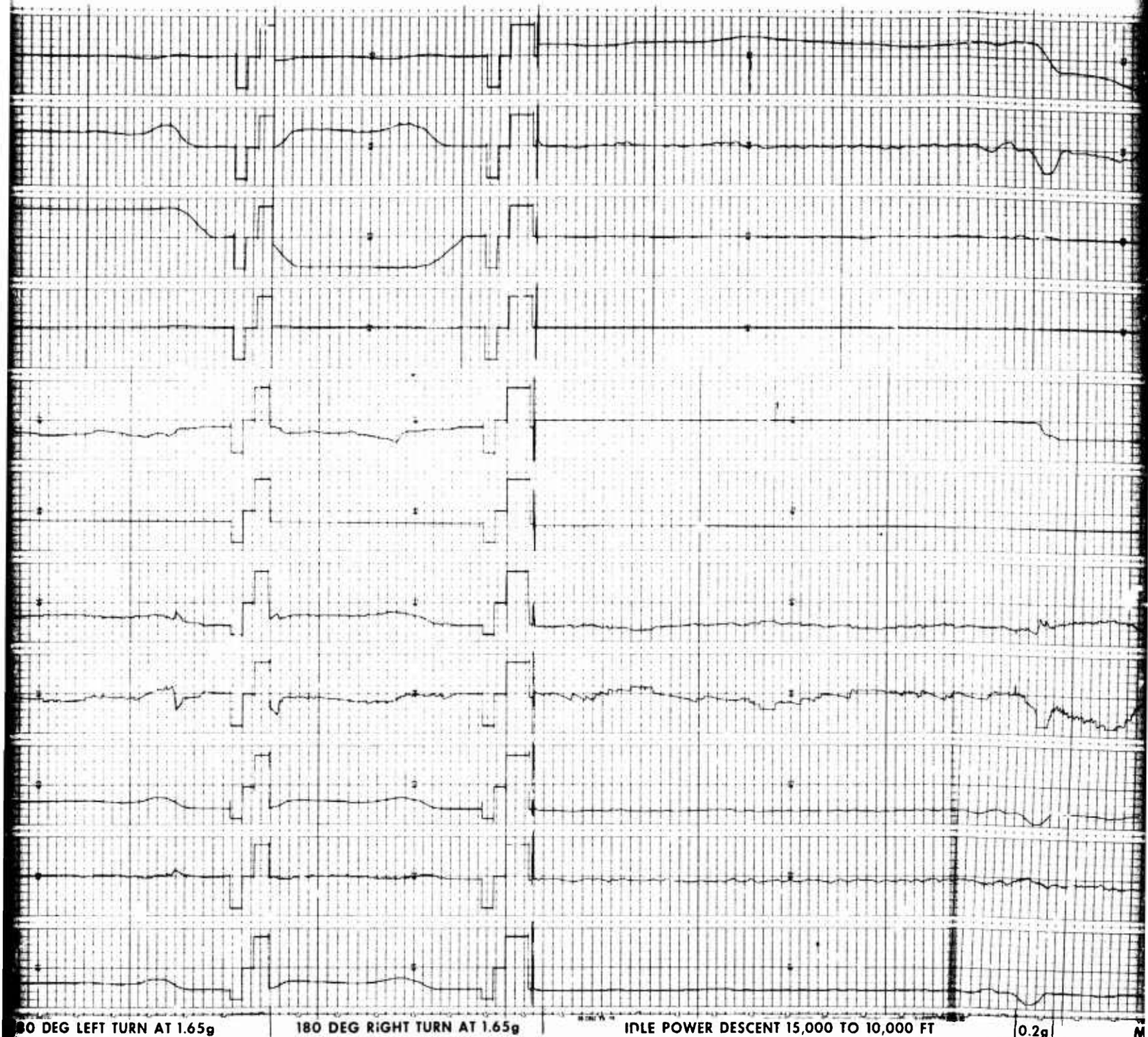
180 DEG LEFT TURN AT 1.65g
180 DEG RIGHT TURN AT 1.65g
IDLE POWER DESCENT 15,000 TO 10,000 FT
0.2g
PUSH OVER

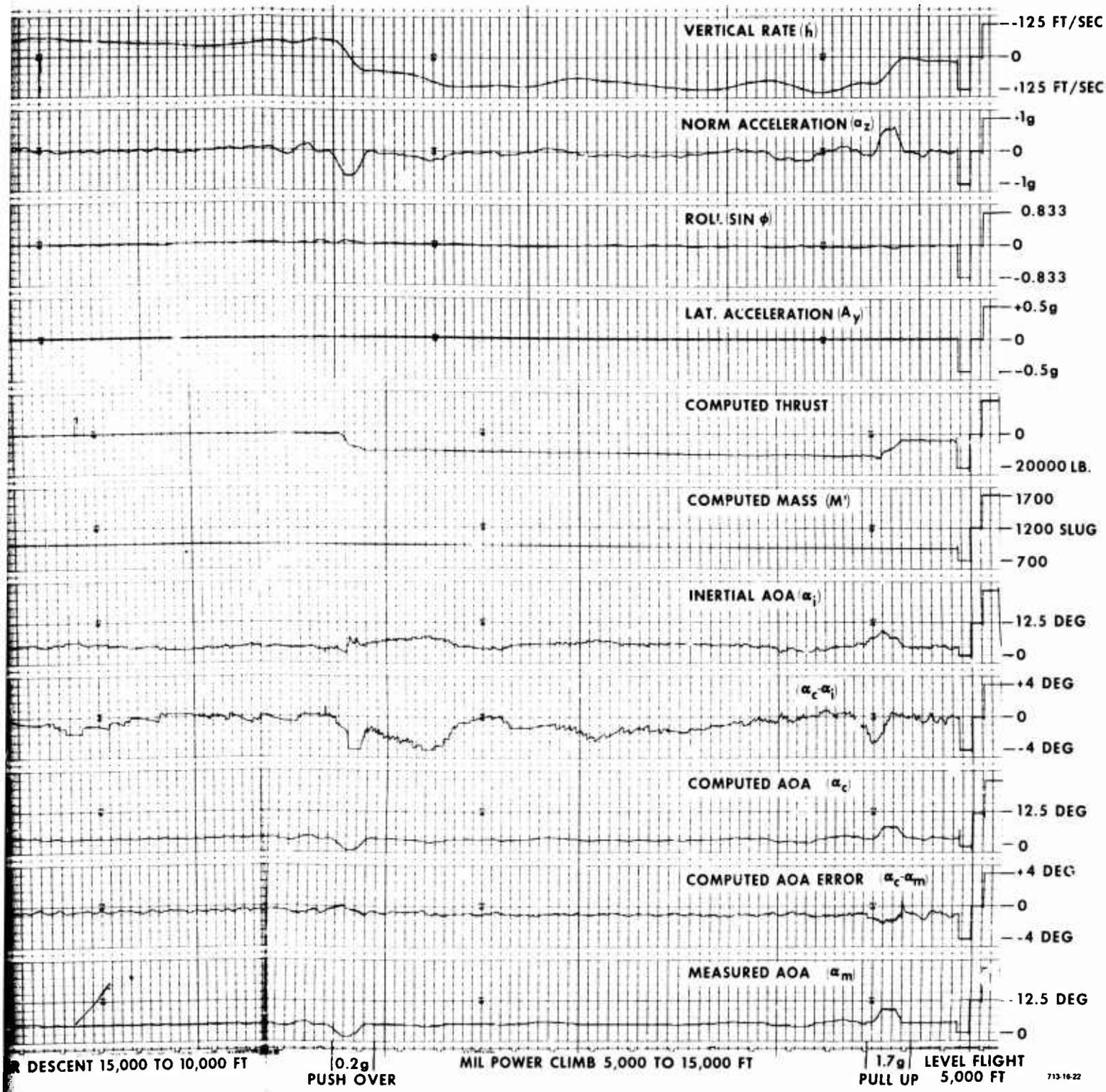

Figure 22
Dynamic Evaluation, Flaps Retracted - 220 knots

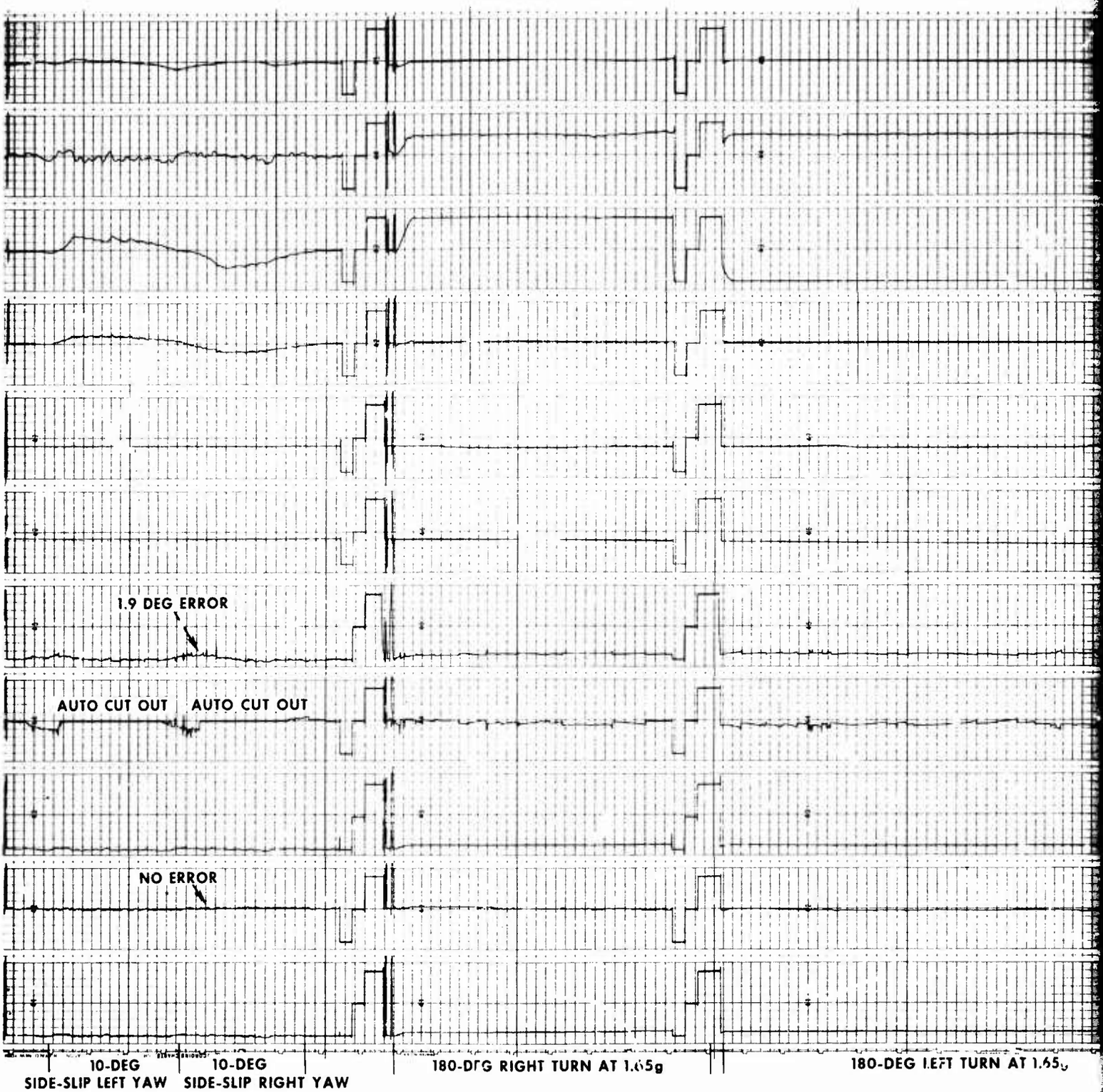
1.9 DEG ERROR
AUTO CUT OUT
AUTO CUT OUT
NO ERROR
10-DEG
SIDE-SLIP LEFT YAW
10-DEG
SIDE-SLIP RIGHT YAW
180-DEG RIGHT TURN AT 1.65g
180-DEG LEFT TURN AT 1.65g

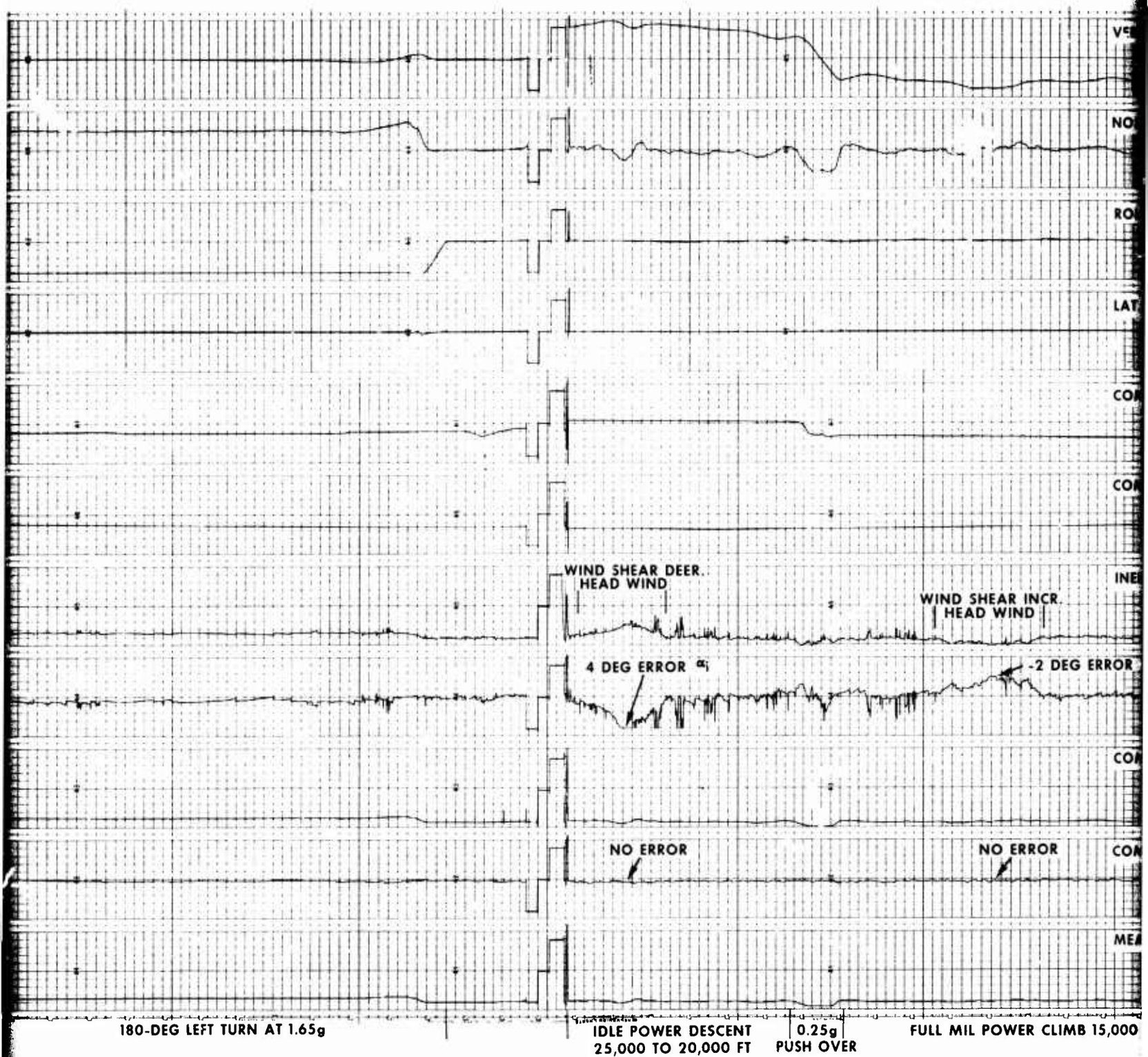

F

Dynamic Evaluation,

4

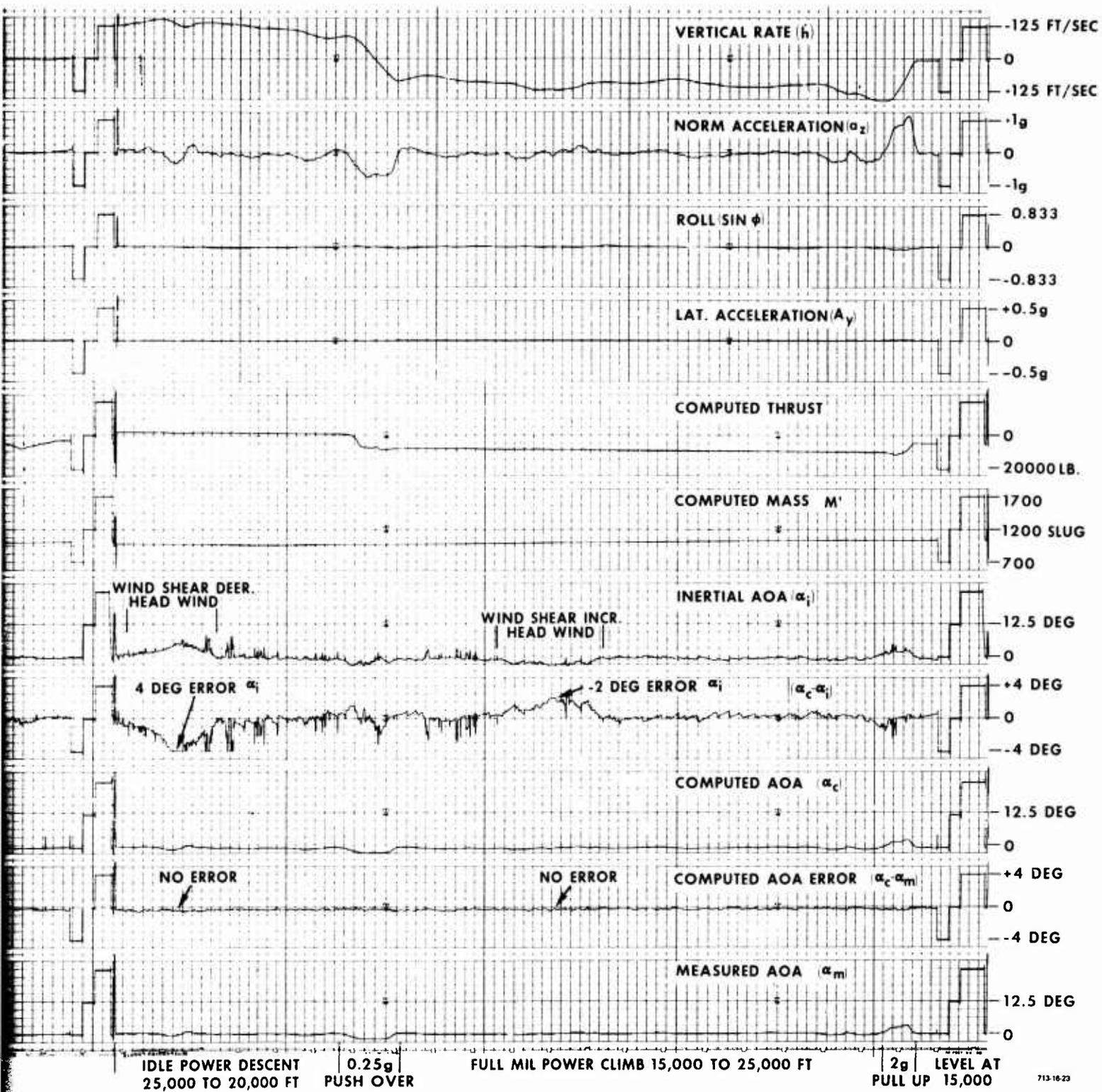

Figure 23
Dynamic Evaluation, Flaps Retracted - 350 knots

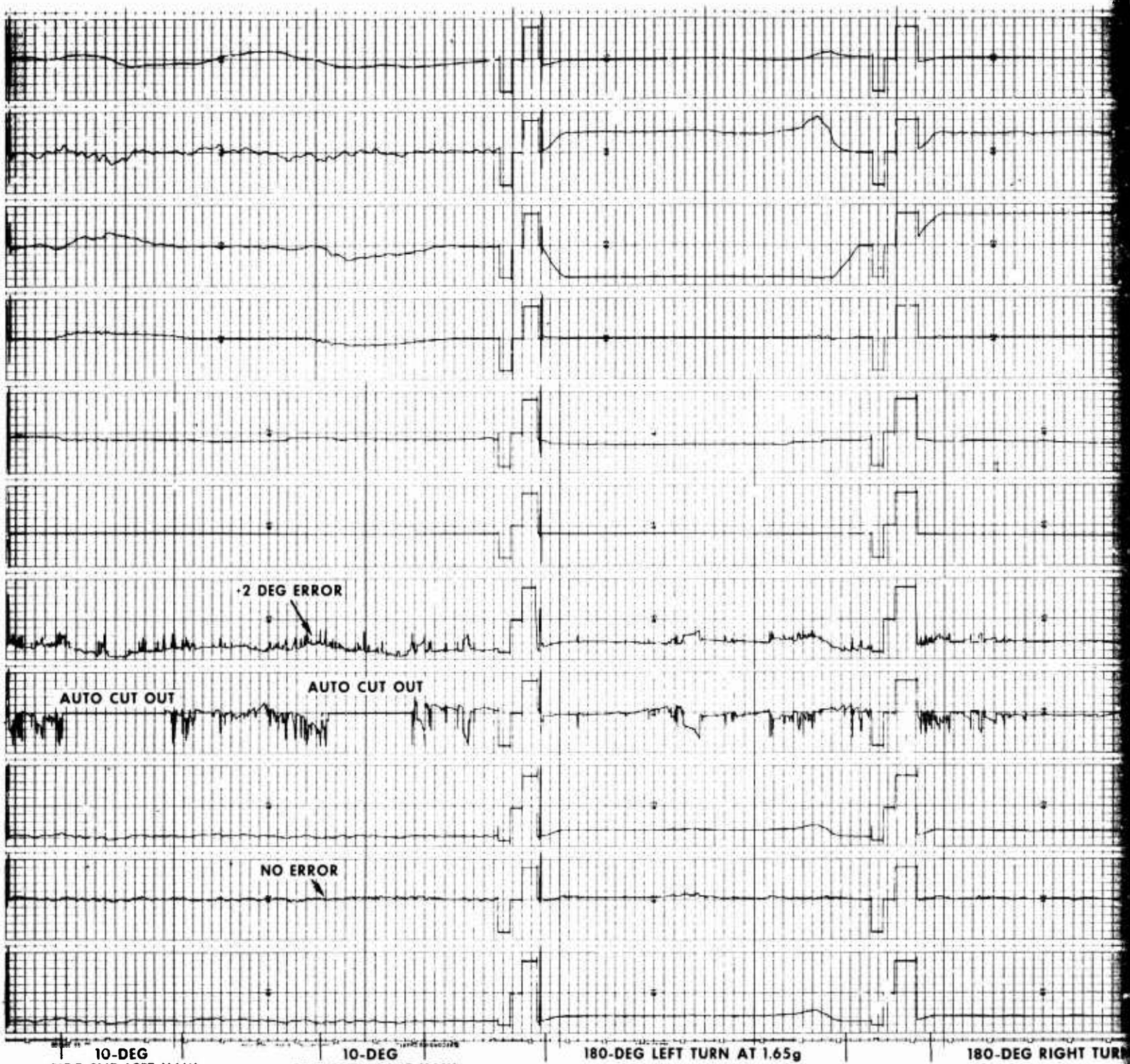
+2 DEG ERROR
AUTO CUT OUT
AUTO CUT OUT
NO ERROR
10-DEG
SIDE-SLIP LEFT YAW
10-DEG
SIDE-SLIP RIGHT YAW
180-DEG LEFT TURN AT 1.65g
180-DEG RIGHT TURN

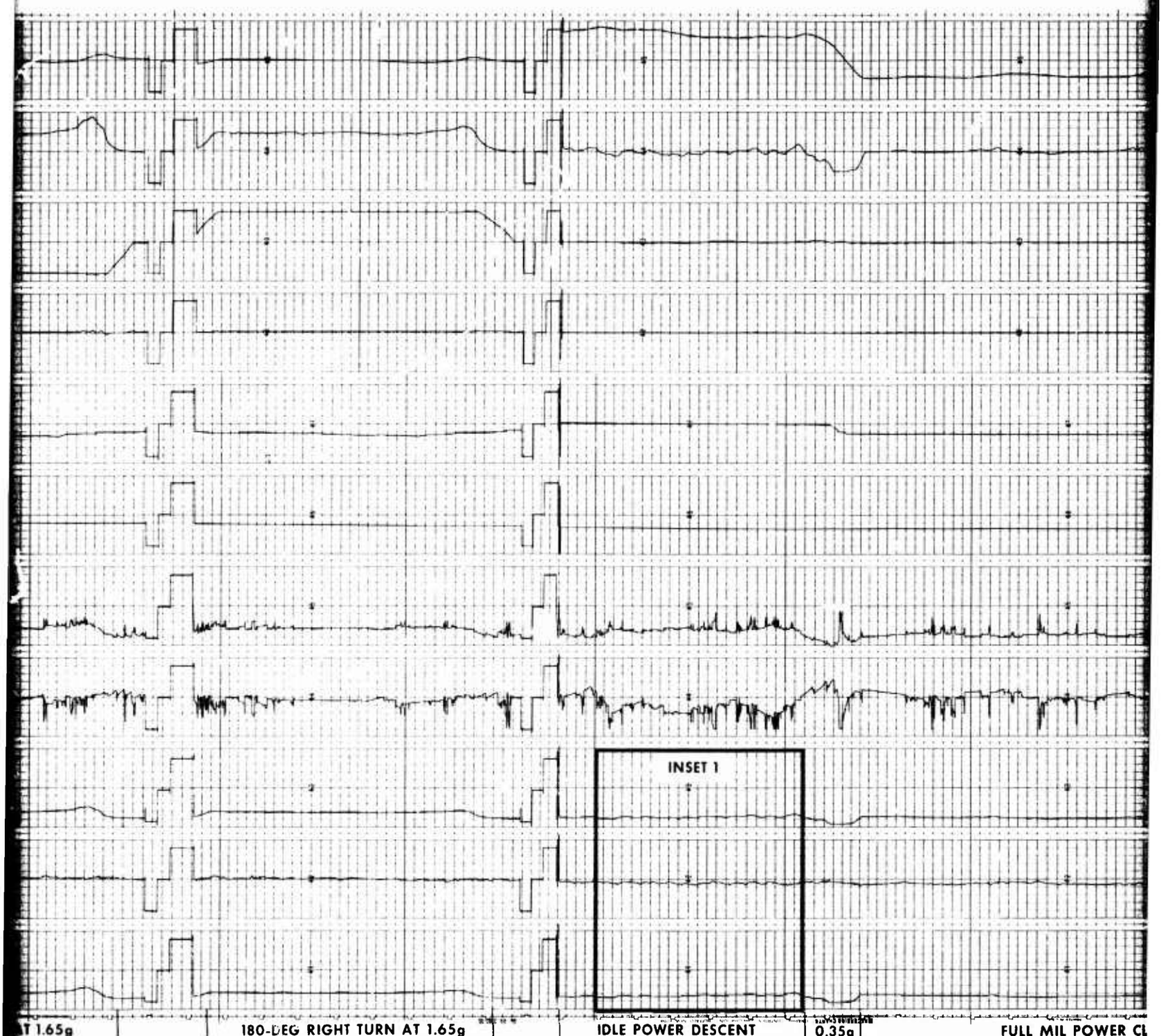
INSET 1
T 1.65g
180-DEG RIGHT TURN AT 1.65g
IDLE POWER DESCENT
35,000 TO 30,000 FT
0.35g
PUSH OVER
FULL MIL POWER CL

Dyn

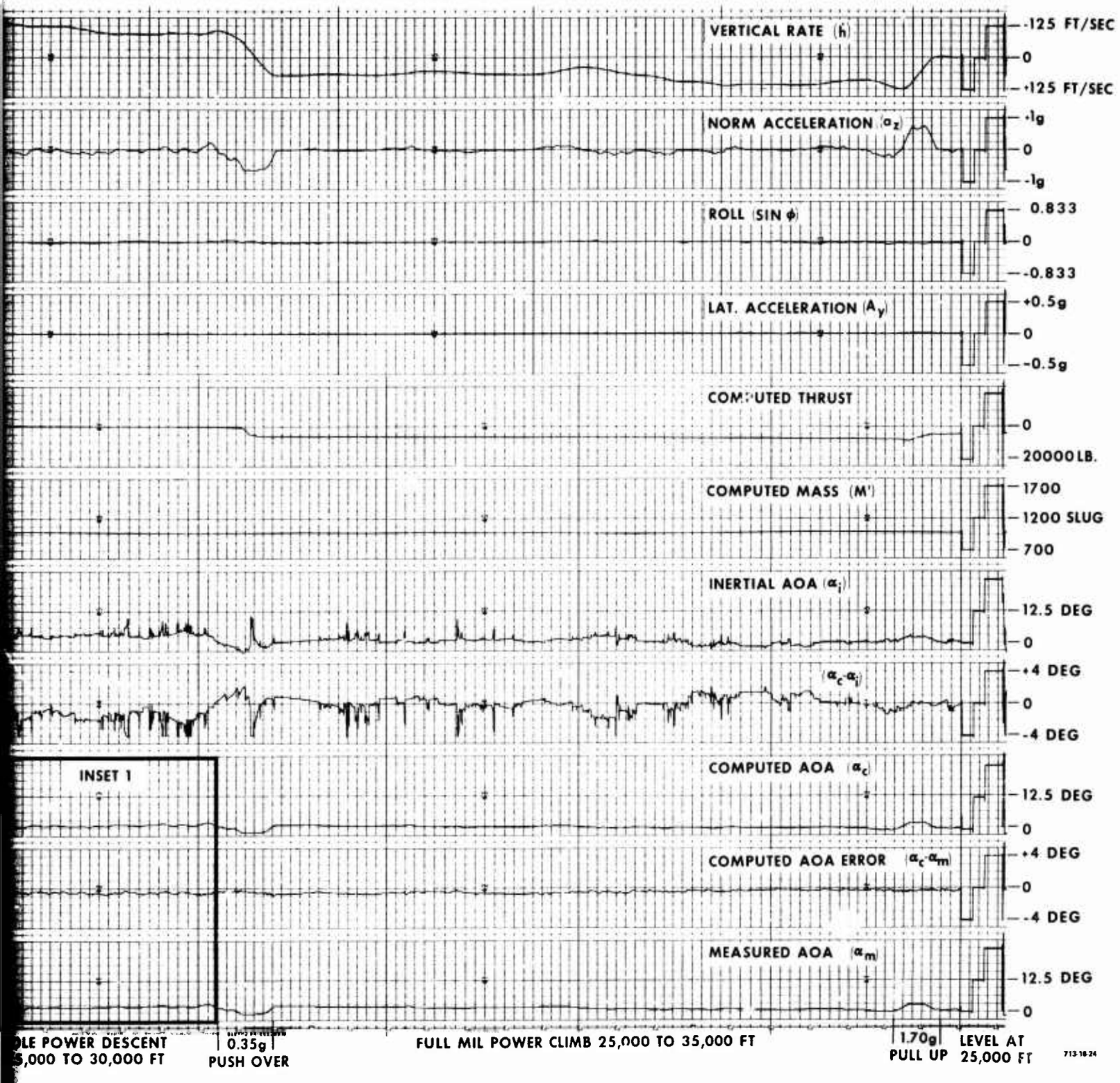

Figure 24
Dynamic Evaluation, Flaps Retracted - 0.75M

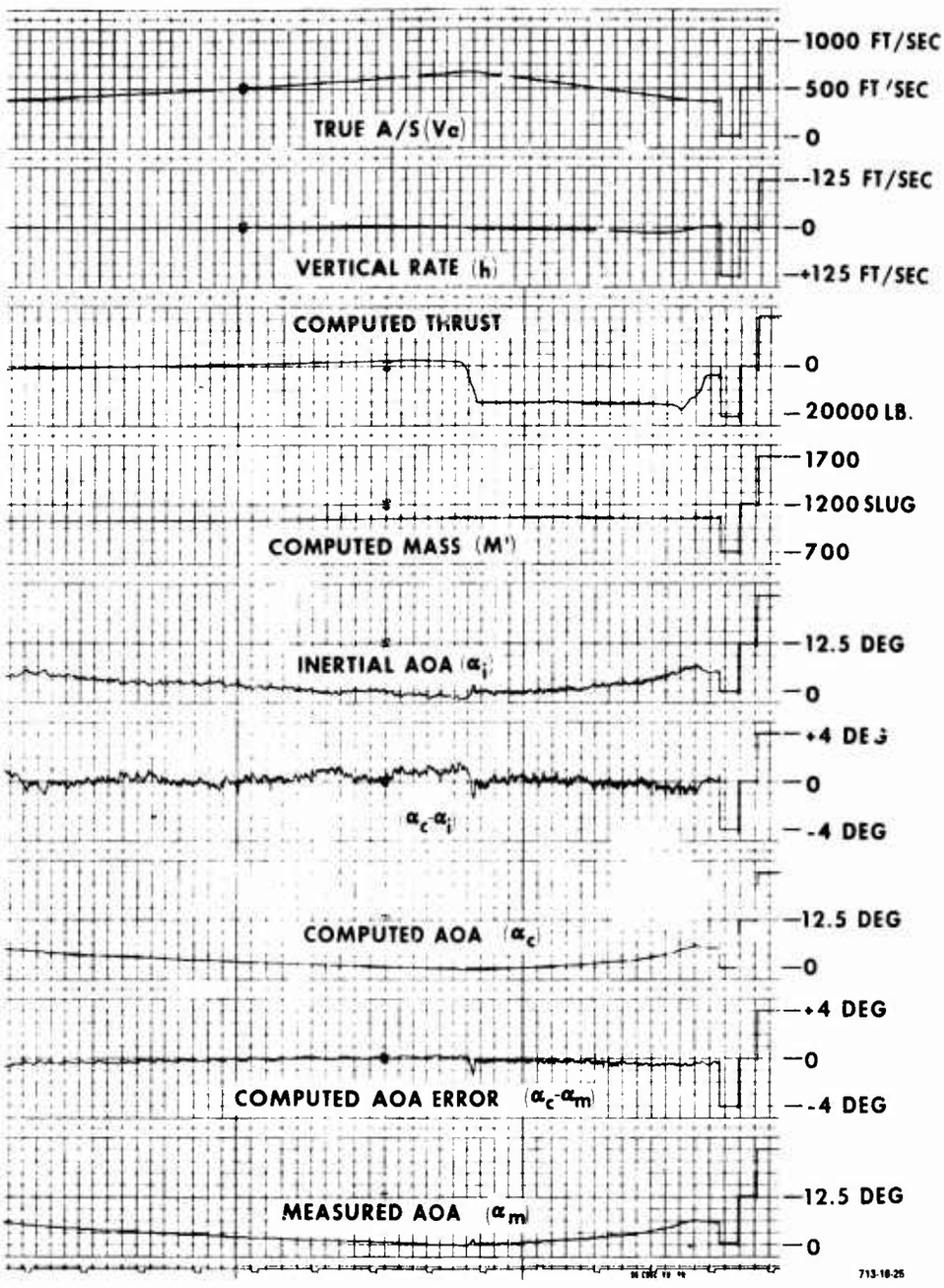

Figure 25
Dynamic Evaluation, Acceleration/Deceleration

MEASURED ERROR

Feet	Flaps	Knots	Degree Maximum	Figure
2,000	1/2	190	1.0*	21
5,000	0	220	0.5**	22
15,000	0	250	0.2	23
25,000	0	0.75M	0.0	24

b. 0.2g to 0.35g Pushover Maneuver

Results here were generally better than in the pull-up maneuver.

MEASURED ERROR

Feet	Flaps	Knots	Degree Maximum	Figure
6,000	1/2	190	0.5	21
15,000	0	220	0.4	22
25,000	0	350	0	23
35,000	0	0.75M	0.1	24

c. Full Mil Power Climb/Idle Power Descent

Comparison of the climb to the descent would tend to produce an angle-of-attack error which might result from error in flight path angle or error in calculated thrust. No error change is discernible between the climb segment and descent segment.

d. Windshear Disturbance

The ability of the angle-of-attack processor to ignore windshear and turbulence is shown in Figure 23. At approximately 23,000 feet, a disturbance in inertial angle-of-attack (α_i) builds up to a -2 degree error while α_M and α_c are undisturbed. Presumably the error is caused by an increase in headwind as the aircraft passes through that level. Computed angle-of-attack (α_c) completely rejects this disturbance and shows no error.

The same disturbance is seen in the descent, but in reverse as headwind decreases passing through the 23,000-foot level. In this instance, there is a +4 degree error in α_i while the angle-of-attack processor output (α_c) is undisturbed.

e. 180-degree Left and Right Turns at 1.6g to 1.8g
(Bank Angle Approximately 55 Degrees)

In these maneuvers the computed alpha proves to be quite accurate. The small errors measured from the data are questionable considering the evaluation system errors.

HIGH BANK ANGLE TURN ERROR

Knots	Flaps	Error Maximum (deg)	Figure
180	1/2	0.8	21
220	0	0.3	22
350	0	0.2	23
0.75M	0	0.2	24

*Estimated - Noise tends to obscure valid data.
**Neglecting severe sticking of α_M vane.

f. Side-Slip Maneuvers

These maneuvers demonstrate the accuracy of computed angle-of-attack in moderate side-slip angles of approximately ±10 degrees.

It is clearly apparent that the inertial alpha (α_I) is very sensitive to side-slip, but that the angle-of-attack processor output (α_C) derived from aircraft mass is not. Error is barely detectable and only at the low speeds.

g. Accelerate/Decelerate Maneuver

To evaluate performance during changing speed flight the following test was conducted. While holding altitude at 15,000 feet with the flaps retracted, apply full mil power and accelerate from 220 to 370 knots IAS. Then reduce power to idle and decelerate to 220 knots IAS.

Data from this test is presented in Figure 25. Here again, the -0.5-degree error at low speeds is evident with error reducing to near zero at the high speed. There is no apparent error introduced as a result of acceleration or thrust per se. A 1-degree spike is seen on the vane alpha trace α_M, but it is believed a power transient might have been the cause. That response was not characteristic of the vane.

REFERENCES

1. AEEC Letter No. 702-40, July 17, 1970, "Circulation of Proposed Wind Model------."